Cerebrovascular reactivity (CVR) MRI with CO2 challenge: a technical review

Peiying Liu[a,*], **Jill De Vis**[a], and **Hanzhang Lu**[a,b,c]

[a]Department of Radiology, Johns Hopkins University School of Medicine, Baltimore, MD 21287

[b]Department of Biomedical Engineering, Johns Hopkins University School of Medicine, Baltimore 21287

[c]F.M. Kirby Center for Functional Brain Imaging, Kennedy Krieger Institute, Baltimore, MD 21205

Abstract

Cerebrovascular reactivity (CVR) is an indicator of cerebrovascular reserve and provides important information about vascular health in a range of brain conditions and diseases. Unlike steady-state vascular parameters, such as cerebral blood flow (CBF) and cerebral blood volume (CBV), CVR measures the ability of cerebral vessels to dilate or constrict in response to challenges or maneuvers. Therefore, CVR mapping requires a physiological challenge while monitoring the corresponding hemodynamic changes in the brain. The present review primarily focuses on methods that use CO2 inhalation as a physiological challenge while monitoring changes in hemodynamic MRI signals. CO2 inhalation has been increasingly used in CVR mapping in recent literature due to its potency in causing vasodilation, rapid onset and cessation of the effect, as well as advances in MRI-compatible gas delivery apparatus. In this review, we first discuss the physiological basis of CVR mapping using CO2 inhalation. We then review the methodological aspects of CVR mapping, including gas delivery apparatus, the timing paradigm of the breathing challenge, the MRI imaging sequence, and data analysis. In addition, we review alternative approaches for CVR mapping that do not require CO2 inhalation.

1. Introduction

Cerebrovascular reactivity (CVR) denotes the ability of cerebral vessels to dilate or constrict in response to challenges or maneuvers. This physiological parameter is thought to be an

---

[*]Corresponding author: Peiying Liu, Ph.D., Department of Radiology, Johns Hopkins University School of Medicine, 600 N. Wolfe Street, Park 324, Baltimore, MD 21287, peiying.liu@jhu.edu, Phone: 410-955-4173, Fax: 410-614-1977.

important index of the brain's vascular health, and provides vascular reserve information that is complementary to steady-state vascular parameters, such as cerebral blood flow (CBF) and cerebral blood volume (CBV). In recent years, there has been a surging interest in the measurement of CVR in a range of applications. The potential clinical utility of CVR mapping includes arterial stenosis (De Vis et al., 2015b; Donahue et al., 2013; Gupta et al., 2012; Mandell et al., 2008; Mikulis et al., 2005), stroke (Geranmayeh et al., 2015; Krainik et al., 2005), small vessel disease (Greenberg, 2006; Marstrand et al., 2002), brain tumors (Fierstra et al., 2016; Pillai and Zaca, 2011; Zaca et al., 2014), traumatic brain injury (Chan et al., 2015; Kenney et al., 2016), substance abuse (Han et al., 2008), and normal aging (De Vis et al., 2015a; Gauthier et al., 2013; Lu et al., 2011). CVR has also been utilized to calibrate or normalize functional MRI (fMRI) signals to obtain a more quantitative measure of task-induced changes in neural activity (Davis et al., 1998; Hoge et al., 1999; Kannurpatti and Biswal, 2008; Liu et al., 2013a; Liu et al., 2013b; Restom et al., 2008; Song et al., 2016; Tsvetanov et al., 2015). More details of the applications for CVR can be found in other articles in this special issue.

The goal of the present article was to provide a review of the technical aspects of CVR mapping using MRI. CVR mapping is different from other perfusion imaging techniques in that a physiological challenge is usually required during the MRI scan. The present review will primarily focus on methods that use CO2 inhalation as a physiological challenge while monitoring changes in hemodynamic MRI signals. CO2 inhalation has been increasingly used in recent literature due to its potency in causing vasodilation, rapid onset and cessation of the effect, as well as recent advances in MRI-compatible gas delivery apparatus. In this review, we will first discuss the physiological basis of CVR mapping using CO2 inhalation. We will then review the methodological aspects of CVR mapping, including gas delivery apparatus, the timing paradigm of the breathing challenge, the MRI imaging sequence, and data analysis. In addition, we will review alternative approaches for CVR mapping that do not use CO2 inhalation.

2. Physiological basis of CVR measurement using hypercapnia challenge

Figure 1 illustrates the molecular mechanisms of vasodilation during hypercapnia challenge (i.e., an elevation of the body's CO2 level due to challenges such as CO2 inhalation). Hypercapnia-induced relaxation of vascular smooth muscle cells (SMCs) in the arteries is caused by an increase in CO2 content of the interstitial compartment and in the endothelial cells. Increased CO2 content results in a decrease in pH through the formation of carbonic acid, followed by its dissociation into proton (H^+) and bicarbonate ions (HCO_3^-) (Yoon et al., 2000). Both the increased CO2 and decreased pH can lead to SMC relaxation, and consequently, vasodilatation, through mechanisms we briefly discuss below.

CO2 and pH have a direct effect on SMC. Both increased interstitial CO2 and decreased interstitial pH can open potassium (K^+) channels on the SMCs (Brayden, 1996; Peng et al., 1998), resulting in hyperpolarization of the SMCs. SMC hyperpolarization decreases the activity of voltage-dependent calcium (Ca^{2+}) channels, and thus, reduces intracellular Ca, which leads to vasodilatation.

CO2 and pH can also indirectly dilate SMCs through their effects on the vascular endothelia. Increased CO2 and decreased pH can cause hyperpolarization of the endothelial cells through K-channels, which, in turn, alters the membrane potentials of the SMCs via myo-endothelial gap junctions that transport negative charges of the endothelium cells to the SMCs (Sandow et al., 2009). CO2 and pH can also cause activation of nitric oxide synthase (NOS) in the endothelia (Fathi et al., 2011; Xu et al., 2004; Ziegelstein et al., 1993). Activation of NOS increases the concentration of nitric oxide (NO). NO then diffuses into the SMCs and results in the relaxation of SMCs (Bolotina et al., 1994; Zhao et al., 2015).

3. Gas delivery

Delivery of a special gas mixture to a subject inside the MRI scanner is not a trivial task. Special considerations with regard to the gas delivery system include: 1) all components inside an MRI room must be MRI-compatible; 2) the breathing apparatus should work within the small space that the MRI system and its head coil allow; 3) the breathing apparatus should work with the patient in a supine position, which the MRI requires, and should cause minimal discomfort; and 4) the inspired gas type needs to be adjustable while scanning without causing any subject motion. Several gas delivery systems have been proposed in the literature. They can be broadly grouped into two categories: fixed inspired CO2 and fixed expired CO2 systems.

3.1 Fixed CO2 concentration in the inspired gas

This type of systems delivers room air to the subjects at the baseline state and hypercapnic gas with a fixed CO2 concentration (e.g., 5% CO2 with 21% O2 and balanced N2) at the challenged state.

Figure 2a shows the diagram of a representative gas delivery system (Lu et al., 2014; Yezhuvath et al., 2009). In this system, the pre-mixed hypercapnia gas (e.g., 5% CO2, 74% N2, and 21% O2) is contained in a large Douglas bag, e.g., 100 liters, that is pre-inflated and brought into the magnetic room. The gas is delivered to the subject through a mouthpiece where the inspired and expired air flows through different ports of a non-rebreathing valve, thus avoiding mixing between them. During the MRI scan, the subject wears a nose-clip and is instructed to breathe through the mouthpiece. End-tidal CO2 (Et-CO2) is sampled near the mouthpiece. A researcher stays inside the magnet room throughout the experiment to manually switch the valve to control the inspired air (either room air or CO2 bag) and to monitor the subject.

In another system, a facemask is used instead of a mouthpiece (Figure 2b) (Lajoie et al., 2016; Tancredi et al., 2014). The advantage of the facemask is that the subject can maintain nose breathing, and thus, does not experience dry mouth during the scan. However, the facemask tends to require more space compared to the mouthpiece and may require more effort to fit in the head coil of the MRI, especially multi-array-type coils that are usually smaller in size. The Tancredi system is also different from the Lu system in that the gas mixture is delivered to the subject via a gas tank rather than a Douglas bag. The benefit of the gas tank delivery is that the incoming air is pressurized, and thus, there is less mechanical resistance in the delivery system and less effort is needed on the subject's part to

inhale the air. One disadvantage is that the gas flow rate needs to be optimized per subject based on their ventilation rate and, when a fixed rate is used, an additional outlet port of a sufficient length (e.g., 3.5 m) is necessary to serve as a gas reservoir. A similar system, with manual control of flow meters, has also been reported recently (Driver et al., 2016; Whittaker et al., 2016).

Another variant of the fixed inspired CO2 system is shown in Figure 3c (Bulte et al., 2009; Hare et al., 2013). Compared to the other two, this system does not use a non-rebreathing valve to explicitly avoid the mixing of inspired and expired air. Instead, it employs an excessive flow rate in the incoming air, e.g., twice the amount of the ventilation rate, to quickly dilute the expired air and minimize rebreathing. The absence of a non-rebreathing valve with this setup is expected to reduce the effort needed during inhalation. However, greater effort may be required for exhalation because of the high-pressure incoming air. In addition, for gas systems that use tanks, the tanks usually need to be moved in and out of the MRI suite for every study, which is less convenient compared to moving a Douglas bag.

Common features of the fixed inspired CO2 systems are that they tend to be less expensive, involve less training and preparation for both the researcher and the participant, and troubleshooting is simpler. A potential limitation is that there may be some variations in baseline Et-O2 and challenge-induced Et-CO2 changes across subjects, due to individual differences in ventilation.

3.2 Fixed CO2 concentration in the expired gas

This type of systems uses feedback control or individualized pre-calibration to ensure that the expired CO2 level of the participant is maintained at desired levels. Two such systems have been reported thus far for use in MRI experiments (Slessarev et al., 2007; Wise et al., 2007).

One system (Wise et al., 2007) uses a gas-mixing chamber where five gases (pressured air, O2, CO2, N2, and a backup O2) are mixed under the control of a laptop computer. The mixed gas is delivered to the subject's face-mask at a constant rate, e.g., 70 liters per minute, and the exhaled air is sampled and Et-CO2 is measured. The controlling computer compares the desired Et-CO2 value with the measurements, and then, through feedback control, modifies the CO2 content in the mixed gas on a breath-by-breath basis, thereby ensuring a fixed CO2 level in the expired air.

Another system of fixed expired CO2 (Slessarev et al., 2007) achieves a targeted CO2 level by exploiting the fact that the expired CO2 level is directly related to the ventilation volume, when the inspired CO2 and the body's metabolic production of CO2 are known. Therefore, by controlling the "effective" ventilation volume of the subject, the expired CO2 level can be fixed. Unlike the fixed inspiration systems that avoid rebreathing, this system utilizes the previously exhaled gas in addition to the incoming gas for the subject's ventilation needs. Specifically, the volume of incoming fresh air is determined by the "effective" ventilation volume that the researcher determined during a preparation step. Then, any additional volume that the subject needs is met through rebreathing the exhaled air, which does not contribute to CO2 removal. The advantage of this system is that feedback control is not

required, which simplifies the system. However, the preparation time for each study is relatively long and substantial training of the subject is needed to ensure a successful targeting of expired CO_2.

Compared to the fixed inspired CO_2 systems, an advantage of the fixed expired systems is that they allow precise control of exhaled CO_2 across different subjects and, since brain hemodynamic response is directly related to the exhaled CO_2 content rather than inhaled CO_2, this scheme can potentially provide more harmonized data compared to the fixed inspired CO_2 method. However, these systems are often expensive, require more training of the operators, and take a longer time to set up for each study. Furthermore, because of the CO_2 targeting, the baseline CO_2 level under which the measurement is performed is no longer the natural baseline CO_2 level that the subject's body usually operates under. Thus, it remains to be shown whether the measured CVR is relevant to the subject's vascular health in daily functioning.

To date, there has been no study that has systematically compared these gas delivery systems in the same patients. The selection of a specific gas delivery system is often based on factors such as the study requirement (Fierstra et al., 2013), the project budget, and the skills of the personnel, for which a consensus for the field would be desirable.

4. Measurement of CO2 time course

Regardless of the type of breathing system used, the measurement of Et-CO_2 is an important component in a CVR experiment in order to accurately assess CVR, as this physiological parameter signifies the extent to which the vascular system is challenged, i.e., the strength of the stimulus. Et-CO_2 denotes the maximal concentration of CO_2 in the exhaled air. It is a surrogate of alveolar carbon dioxide (PaCO_2), the change of which leads to vasodilation or restriction. Et-CO_2 is usually 2–5 mmHg lower than PaCO_2 in healthy adults (Nunn and Hill, 1960), as about 1–2% alveoli are not participating in gas exchange in the lung, and thus, the air inside these alveoli dilutes CO_2 in the exhaled air (Bhavani-Shankar et al., 1995; Fletcher et al., 1981). The volume of these poorly perfused alveoli, referred to as alveolar dead space, accounts for about 5–10% of the tidal volume in healthy adults (Williams et al., 1997) and varies with age and clinical situations (Askrog, 1966; Burrows, 1989; Yamanaka and Sue, 1987). Although Et-CO_2 could be lower than PaCO_2, a strong correlation between Et-CO_2 and PaCO_2 has been reported (McSwain et al., 2010; Peebles et al., 2007; Sullivan et al., 2005). Therefore, Et-CO_2 is considered a surrogate, non-invasive approximation of PaCO_2.

If a sampling tube is placed near the mouthpiece or facemask of the breathing system to measure the CO_2 content in the sampled air, the typical time course of such a recording is shown in Figure 3. Each fluctuation period of the time course represents a respiratory cycle, with the lower peaks of the trace indicating CO_2 content in the inhaled air and the upper peaks indicating CO_2 content in the exhaled air, i.e., Et-CO_2. The signal transition between the lower and upper peaks represents the mixing of inhaled and exhaled air. As can be seen in Figure 3a, during room-air breathing, the bottom of the signal is approximately zero because there is virtually no CO_2 in the inhaled room air. The upper peak of the signal is

approximately 40 mmHg, which is typical of Et-CO_2 for a healthy volunteer. During the hypercapnia breathing period, the trough of the signal is 38 millimeter of mercury (mmHg), which is consistent with the CO_2 content in the inhaled air of 5% of atmospheric pressure (760 mmHg). The Et-CO_2 during hypercapnia is typically 8–12 mmHg above the value during room-air breathing.

The device to measure Et-CO_2 is generally referred to as a capnograph monitor. Some capnograph monitors provide only Et-CO_2, rather than the complete CO_2 tracer, as outputs. While the Et-CO_2 curve is, in principle, sufficient for CVR measurement, such monitors often fail to give valid Et-CO_2 values during the transition periods of the experiment, e.g., from room air to hypercapnic gas (see inset of Figure 3a). This is because these monitors rely on a built-in algorithm to extract Et-CO_2 from the complete CO_2 trace, but, unfortunately, the algorithms are designed for a steady-state condition and often do not work for transition periods between normocapnia and hypercapnia. Therefore, capnograph monitors that record only Et-CO_2 values usually miss certain time points and are not suitable for CVR experiments.

Thus, it is recommended to use capnograph monitors that provide recordings of a breath-by-breath trace (e.g., those shown in Figure 3a) of CO_2 concentration at a relatively high sampling rate (>40Hz). The Et-CO_2 time course (i.e., the envelope of the CO_2 concentration time course) can then be extracted by off-line processing of the recorded CO_2 traces. The Et-CO_2 extraction procedure first needs to correct for the tubing delay from the subject's mouth/nose to the CO_2 monitor. Then, the procedure often involves an algorithm that detects the peaks of the CO_2 trace at every breath, followed by interpolation or re-sampling to match the temporal resolution of the MRI data. Manual verification and correction are also commonly applied, in case the algorithm fails to detect the correct peaks during transition periods or when an atypical breathing pattern occurs. Some researchers also perform a temporal filtering (Yezhuvath et al., 2009) or a polynomial fitting (Tancredi et al., 2014) to the CO_2 peaks to account for dispersion of the gas bolus when traveling from the lung to the brain.

It is also useful to note that, under most circumstances, the exhaled CO_2 concentration is higher than the inhaled CO_2; thus, Et-CO_2 is represented by the upper peak of the CO_2 recording. However, this may not be the case when a high concentration of CO_2 gas is used in the experiment. Figure 3b shows a CO_2 recording when the inhaled gas is changed from room air to 7.5% CO_2. It can be seen that, during the hypercapnic period, the inhaled gas actually contains more CO_2 then the exhaled gas. Consequently, during that period (blue arrows in Figure 3b), Et-CO_2 is represented by the lower peaks of the CO_2 recording. After the inhaled gas is switched back to room air, Et-CO_2 is, again, indicated by the upper peak. This example further underscores the importance of obtaining a complete CO_2 recording during the experiment.

5. CO_2 inhalation paradigm

For fixed inspired CO_2 experiments, the block paradigm is the most widely used CO_2 inhalation paradigm in the literature. A typical block-designed paradigm is shown in Figure

4a. In this paradigm, room air and hypercapnic gas are supplied to the subject in an interleaved fashion. The duration of each hypercapnia block varies from 50s (Liu et al., 2017b; Thomas et al., 2013), 60s (Hare et al., 2013; Yezhuvath et al., 2009), and 80s (Mark et al., 2010) to 2.3min (Tancredi and Hoge, 2013). The duration of the room air block is often similar or slightly longer than the hypercapnia block. The block paradigm is easy to implement, and has been widely used in CVR mapping. There are some variations of the block design, such as the graded hypercapnia paradigm, which varies the CO_2 concentration in different blocks (Driver et al., 2010), or the asymmetric block design, which varies the duration of different blocks (Poublanc et al., 2015). Such a non-periodic design could help to distinguish the brain areas that have a prolonged bolus arrival time (e.g., in patients with arterial stenosis) from those who have negative CVR but a regular bolus arrival time.

For experiments with control of expired CO_2, more advanced CO_2 inhalation paradigms have also been proposed, such as a sinusoidal paradigm (Figure 4b) in which Et-CO_2 is modulated in a sinusoidal fashion (Blockley et al., 2011; Blockley et al., 2017; Halani et al., 2015), and a ramp paradigm (Figure 4c) in which Et-CO_2 increases progressively to a targeted level (e.g., 10 mmHg above baseline) within 75s (De Vis et al., 2015a), 120s (Fisher et al., 2017) or longer (Bhogal et al., 2015). These paradigms require a gas delivery system that targets CO_2 concentration in the expired gas.

CVR mapping using non-BOLD pulse sequences, such as quantitative flow phase-contrast MRI or arterial spin labeling (ASL) MRI, often use a step paradigm (Figure 4d). In this paradigm, the subject breathes room air continuously for a few minutes while baseline MRI images are acquired. Then, the subject breathes hypercapnic air for another few minutes (Figure 4d) while the challenge-state images are acquired after the physiology is stabilized (Leoni et al., 2017; Leung et al., 2013; Liu et al., 2012; Zhao et al., 2009). The challenge can be repeated, when necessary, to improve the reliability of the measurements (Mark et al., 2010; Tancredi et al., 2015).

Breathing of hypercapnic gas may cause transient discomfort. Such discomfort can be reduced by lowering the concentration of CO_2 in the inspired gas and shortening the duration of the hypercapnia block. Therefore, the selection of a CO_2 inhalation paradigm should take into account the hypercapnia duration and CO_2 concentration to ensure patient comfort. In terms of typical CO_2 concentration for CVR experiments, although the utilization of higher CO_2 concentrations had been reported in the literature (Ainsworth et al., 2015; Fujishima et al., 1971; Oudegeest-Sander et al., 2014), hypercapnia with 5% CO_2 (fixed inspired CO_2 systems) or a 10mmHg increase in Et-CO_2 (fixed expired CO_2 systems) are the most widely used challenges reported in the literature. In terms of the duration of the hypercapnia block, breathing 5% CO_2 for approximately one minute is expected to cause minimal discomfort or even awareness in participants. It is also useful to note that the repetition of hypercapnia blocks generally do not increase discomfort, as long as the duration of each block is kept relatively short, e.g., 60 seconds. Therefore, if the goal is to apply four minutes of hypercapnia and four minutes of room-air breathing to ensure sufficient signal, the periods should be divided into shorter blocks of, say, one-minute each. In terms of the impact of such a splitting approach on CVR data quality, a previous study showed that a paradigm of four blocks of one-minute CO_2 inhalation (more comfortable)

yielded BOLD-CVR results that were to comparable to those of a four-minute continuous inhalation paradigm (less comfortable) (Yezhuvath et al., 2009). It is also generally accepted that short-duration CO_2 inhalation, e.g., no more than three minutes, has a minimal effect on neural activity and brain metabolism (Chen and Pike, 2010; Jain et al., 2011)), whereas a longer period of hypercapnia, e.g., six minutes, may have a suppression effect (Xu et al., 2011), although more recent literature (Driver et al., 2016) suggests that even breath-by-breath changes in CO_2 could alter neural activity to a small extent.

6. MRI acquisition methods in CVR MRI

MR images are acquired concomitantly with the gas challenge. Three hemodynamic MRI sequences have been used in CVR imaging: blood-oxygenation-level dependent (BOLD) MRI, arterial spin labeling (ASL) MRI, and quantitative flow phase-contrast (PC) MRI.

BOLD MRI is the most widely used MRI acquisition technique for CVR mapping due to its superior sensitivity (similar to the situation in the fMRI field). Typical BOLD sequences in the CVR literature use gradient echo echo-planar-imaging (EPI) acquisition. Table 1 shows an example of the BOLD CVR imaging protocol. It should be noted that, since CO_2 inhalation is a global challenge and its hemodynamic responses have several different features than those during brain activation, the optimal sequence parameters for CVR mapping may be slightly different from those of fMRI. For example, it has been reported that, when using a standard fMRI BOLD protocol as mentioned above, negative CVR values were observed in ventricle regions (Blockley et al., 2011; Thomas et al., 2013). This is attributed to the combined effect of the hyperintense CSF signal in typical BOLD images and a CSF partial-volume reduction during hypercapnia, presumably secondary to a CBV increase as a result of dilation of vessels in the choroid plexus (Thomas et al., 2013). This effect is seen only in CVR mapping, but not in fMRI studies, due to the global nature of CO_2 responses. It was also shown recently that, by using a shorter TE (e.g., 21ms), the signal intensity discrepancy between CSF and blood can be reduced and negative CVR can be minimized (Ravi et al., 2016b). Another recent advance in BOLD acquisition is fast imaging methods, such as simultaneous multi-slice (SMS) or multiband (MB) acquisition, which allows CVR image acquisition at a higher temporal resolution. Compared to conventional BOLD, SMS BOLD acquisition has been shown to considerably improve the sensitivity (in Z statistics) of the CVR results (Ravi et al., 2016a). With the enhanced sensitivity, CVR mapping at higher resolution is feasible. Figure 5 shows CVR maps acquired with increasing resolutions from 3.3 mm to 2.0 mm in voxel size.

A limitation of BOLD MRI is that its signal reflects a complex interplay among several hemodynamic and metabolic parameters, including CBF, CBV, cerebral metabolic rate of oxygen, and hematocrit. Although a significant correlation has been reported between BOLD-CVR and CBF-CVR measured by positron emission tomography (PET) (Rostrup et al., 2000), a non-linear relationship has been reported between blood CO_2 content and BOLD signal changes (Bhogal et al., 2014; Halani et al., 2015; Sobczyk et al., 2014). To obtain a more quantitative, less complex measure of CBF response to hypercania, ASL MRI can be used in CVR experiments, which provides a direct measurement of CBF. ASL MRI uses RF pulses and magnetic field gradients to non-invasively label water protons in the

arterial blood, and employs a post-labeling delay to allow the labeled protons to reach brain tissue, at which time an image is acquired. A control image is also acquired, the subtraction of which from the labeled image cancels out signals from static protons and yields a CBF-weighted image. Typical ASL imaging resolution reported in the CVR literature is slightly lower than that used in BOLD CVR studies, and requires more time to acquire one image (usually 6–8 s are needed to acquire one pair of control and labeled images). Table 1 displays an example of the ASL CVR protocol. Compared to BOLD MRI, the main limitation of ASL is that this technique has a much lower signal-to-noise ratio (SNR). Moreover, ASL-based CBF may be confounded by changes in bolus arrival time and labeling efficiency, due to changes in blood flow velocity during hypercapnia. It has been reported that, with 5% CO_2 inhalation, bolus arrival time to brain tissue could be shortened by 5–13% (Donahue et al., 2014b; Ho et al., 2011; Su et al., 2017), and labeling efficiency is also reduced significantly (Aslan et al., 2010; Heijtel et al., 2014). These factors could lead to inaccurate quantification of CVR.

To obtain CBF quantification with higher SNR and without the confounding factors mentioned above, PC MRI can be used. PC MRI utilizes the phase of an image to encode the velocity of moving spins, thus achieving a quantitative flow measurement. PC CVR acquisition can be applied on major venous (e.g., superior sagittal sinus) or arterial (e.g., internal carotid and vertebral arteries) vessels. It has the advantages of simplicity and accuracy in absolute CBF quantification, as well as relatively high reliability. An example of the PC CVR protocol is shown in Table 1. In healthy adults, CBF-based CVR has been reported to be 3–6% CBF change per mmHg of Et-CO_2 change using ASL (Aslan et al., 2010; Bulte et al., 2012; De Vis et al., 2015a; Gauthier et al., 2013) and PC MRI (Caputi et al., 2014; Leung et al., 2013; Xu et al., 2011). For arterial CBF measures, the coefficient-of-variation (CoV) of PC MRI was found to be 2.8% (Liu et al., 2013c). This CoV value is considerably lower than that of ASL, which is 4–9.5% (Chen et al., 2011). The disadvantage of the PC CVR technique is that it provides only global blood flow measures in major arteries or veins, but lacks regional information. Nonetheless, although less popular than BOLD and ASL MRI, PC MRI has been used to measure global CVR in a number of studies (Caputi et al., 2014; de Boorder et al., 2004; Leung et al., 2013; Liu et al., 2012; Xu et al., 2011).

7. Data analysis in CVR MRI

CVR is usually defined by the following equation:

$$CVR = \Delta(MRI\ measurement)/\Delta EtCO2, \quad \text{Eq. [1]}$$

where the MRI measurement can be the BOLD signal or the CBF from ASL or PC MRI. For data that have only limited time points, e.g., one time point for room-air breathing and the other time point for CO2 breathing, (MRI measurement) and Et-CO2 can simply be calculated as the difference between baseline and hypercapnic measurements. For data with a large number of time points, more advanced analysis is needed, which is discussed below.

7.1 General linear model assuming a homogeneous bolus arrive time across the brain

This analysis is conceptually similar to that used in task-evoked fMRI, except that the regressor variable is the Et-CO2 time course. Figure 6a shows a flow chart of the processing steps. Before applying the voxel-wise linear model analysis, the Et-CO2 time course is temporally aligned to the MRI signal time course to account for the time it takes for the CO2 gas bolus to travel from the lung to the heart, then to the brain, and elicit a hemodynamic response. This delay time between Et-CO2 and the MRI signal can be determined by shifting the Et-CO2 time course one TR at a time, and, for every shift, calculating the cross-correlation coefficient (CC) between the two time courses. The MRI time course used here is usually based on a large ROI or on the whole brain where the signal is reliable. The shift value that yields the highest CC or smallest residual signal is considered the "lung-to-brain" delay. Typical delay time in young subjects was found to be approximately 15 seconds (Thomas et al., 2014; Yezhuvath et al., 2009). Older individuals tend to have a longer delay (Thomas et al., 2014). Once the Et-CO2 time course is shifted based on the optimal delay, a voxel-wise linear regression is performed:

$$MRI\ signal = \beta_1 \cdot EtCO2 + \beta_2 \cdot t + \beta_0 + \varepsilon, \quad \text{Eq. [2]}$$

where β_1, β_2, and β_0 are estimated coefficients. The term $\beta_2 \cdot t$ is added to account for any linear drift in MRI signal and ε indicates residual error. CVR, in the unit of percent signal change per mmHg of Et-CO2 change, is computed by:

$$CVR = \frac{\beta_1}{\beta_0 + \min(EtCO2) \cdot \beta_1}. \quad \text{Eq. [3]}$$

The term $\min(EtCO2) \cdot \beta_1$ is included in the denominator so that the measured reactivity is in reference to a state corresponding to the baseline Et-CO2, rather than on a non-physiological state of Et-CO2=0. A voxel-wise CVR map is obtained with this procedure. In addition to the MRI signal drift, other factors may also be included in Eq.[2], such as motion factors and other physiological noise. However, caution should be taken when adding factors to the model, as inclusion of factors that are correlated with Et-CO2 time course (e.g., motion due to breathing) may result in an underestimation of CVR.

7.2 General linear model considering voxel-specific bolus arrival time

The strength of the above method is that the algorithm is relatively robust and the computation demand is modest. However, this method relies on the assumption that the "lung-to-brain" delay time is the same for every voxel in the brain, which has recently been called into question. For example, the white matter was found to manifest a substantially longer delay (by 19 seconds), compared to the gray matter, even in healthy subjects (Thomas et al., 2014). Moreover, some studies have also shown that patients with cerebrovascular diseases have a longer delay time in affected regions and that the delay time itself can be a useful index of disease severity (e.g., intracranial stenosis (Christen et al., 2015; Donahue et al., 2016; Liu et al., 2017b)). Therefore, algorithms have been proposed to conduct linear

modeling using a voxel-specific delay time, which can provide an estimation of both CVR and a map of bolus arrival time.

To obtain a voxel-wise map of bolus arrival time (BAT), the most intuitive approach is to extend the ROI method proposed above to voxel-wise analysis, by shifting the Et-CO2 time course relative to the MRI time course of each voxel and determining the time shift that provides the best correlation, using either maximum CC or minimal residual. However, a delay map using such an approach is usually noisy, especially for the white matter and disease-affected areas where the CVR is low. Liu et al. proposed an improved method using a reference MRI signal as an intermediate to determine the voxel-wise CO2 delay (Liu et al., 2017b). In this method (Figure 6b), a reference signal is generated by averaging MRI time courses from a large reference ROI, e.g., whole-brain for healthy volunteers and unaffected brain regions for patients with disease. The voxel-wise time shift between the reference signal and each voxel in the brain is then calculated. The summation of this shift and the time delay between the reference signal and the Et-CO2 time course then gives a voxel-wise BAT map. Compared to directly aligning Et-CO2 to the voxel-wise BOLD signal, the advantages of using the reference signal as an intermediate are that the reference signal is measured in the brain, has accounted for any dispersion of the CO2 bolus, and is measured at the same sampling rate as the voxel-wise signal. Thus, this signal has a higher correlation with the voxel-wise MRI signal. This approach yields more reliable results for voxel-wise maps of bolus delay. Once the voxel-wise delay map is obtained, the Et-CO2 time courses are shifted accordingly and linear regression similar to that described in Eqs. [2] and [3] is used to obtain a CVR map.

An iterative algorithm, dubbed Regressor Interpolation at Progressive Time Delays (RIPTiDe), has also shown promise in calculating the CO2 bolus delay in a voxel-wise fashion (Donahue et al., 2016; Tong et al., 2011). This algorithm (Figure 6c) first examines the temporal cross-correlations between the Et-CO2 time course, referred to as a probe regressor, and the voxel-wise MRI signals. This step results in a preliminary map of bolus delay. Then, MRI signal from each voxel is shifted accordingly, and a principal component analysis (PCA) is applied to the aligned time courses to compute a single time course that accounts for the highest shared variance. This new time course then replaces the Et-CO2 time course as the new probe regressor and the above-described procedure is repeated until convergence. The outcome of this algorithm is a response delay map and an estimated CO2 response waveform, which can then undergo linear regression analysis to estimate CVR. The advantage of this method is that the estimated CO2 response waveform accounts for CO2 bolus dispersion, and, therefore, has a higher correlation with the voxel-wise MRI signal, which improves the estimation of CVR. A potential limitation is that, when the voxel-wise data are noisy, e.g., in patient with a large region of diminished CVR, the algorithm may not converge to the correct delay time.

In addition to temporal delay characterized by bolus arrival time, studies have suggested that the hemodynamic response to blood CO2 changes may be smoother and broader in the white matter and in disease-affected brain regions (Duffin et al., 2015; Poublanc et al., 2015; Thomas et al., 2014). Characterization of this change in hemodynamic response may also be useful and worth investigating.

7.3 Frequency-based analysis

In the previous analyses, the bolus delay time and CVR were computed in separate steps. Frequency-based methods have been proposed to compute these parameters in one analysis. In this type of analysis, the signals are transformed into the frequency domain and the phase and magnitude of the signals are further analyzed. Specifically, the phase of the MRI signals at the CO2 modulation frequency can be used to obtain the timing of the CO2 bolus arrival (Blockley et al., 2011; Blockley et al., 2017; Duffin et al., 2015), and the ratio of the magnitude between CO2 and BOLD signals represents the CVR. These methods are expected to demonstrate excellent performance when the signal waveforms are close to a sinusoid function (Blockley et al., 2011; Blockley et al., 2013). For other types of signal waveforms, however, the power spectrum of the signal of interest is expected to be more widespread and attention will be required to identify the optimal frequency values to include for the best performance (Duffin et al., 2015).

7.4 Computation of functional connectivity from BOLD-CVR data

The primary feature of the BOLD time course in a CVR experiment is that the signal is modulated by hemodynamic responses to blood CO2 changes. However, the signal is also expected to contain spontaneous fluctuations due to neural activity, similar to those in a resting-state fMRI. Therefore, it was recently proposed that, after factoring out signal modulations attributed to the gas challenge (i.e., the term $\beta_1 \cdot EtCO2$ in Eq.[2]), the residual signal (i.e., the term β_0 in Eq.[2]) can be used to analyze functional connectivity (Liu et al., 2017b). Standard tools for resting-state fMRI can be readily applied to the CVR residual signal and both seed-based and independent component analysis (ICA) approaches have been used (Hou et al., 2017). The functional connectivity information can thus be extracted from a CO2-CVR scan without additional cost in scan duration.

8. Tolerability and reliability of CVR mapping

The tolerability of CO2 inhalation inside an MRI scanner has been studied by Spano et al. (Spano et al., 2013). These authors reviewed the experience of 294 patients (9–88 years old) who underwent CVR examinations with CO2-inhalation, and concluded that it is "safe, well tolerated, and technically feasible in a clinical patient population." In a small fraction of participants (11%), transient symptoms, such as shortness of breath and dizziness, were reported, but there were no major complications. Other large-scale CO2-CVR studies also reported no incidence of adverse events (De Vis et al., 2015a; Donahue et al., 2014a; Gauthier et al., 2015; Lu et al., 2011; Merola et al., 2017; Tchistiakova et al., 2014). However, for safety concerns, patients with respiratory failure or pulmonary diseases should be excluded from CO2 challenges (See (Moreton et al., 2016) for more details).

BOLD-based CVR mapping methods have shown good reproducibility with both fixed CO2 inspiration (Ravi et al., 2016b) and targeted Et-CO2 systems (Kassner et al., 2010). The cross-session coefficient of variation (CoV) is about 5–7% (Kassner et al., 2010; Ravi et al., 2016b), while the cross-day CoV is about 7–10% for the BOLD-based methods (Kassner et al., 2010). BOLD-based CVR has also been found to be correlated with ASL-based CVR, using 5% CO2 inhalation (Halani et al., 2015; Hare et al., 2013), although BOLD-CVR was

found to be more sensitive to basal vascular tension than CBF-based CVR (Halani et al., 2015).

9. Techniques beyond CO2 inhalation

9.1 Concomitant CO2 and O2 inhalation

CO2 can be combined with an O2 gas challenge to measure multiple physiological parameters. O2 inhalation can provide an evaluation of venous cerebral blood volume (CBVv) (Blockley et al., 2013; Bulte et al., 2007). Recently, a block-design-based paradigm was proposed to modulate Et-CO2 and Et-O2 concomitantly, but independently, which allows the measurement of CVR and CBVv simultaneously within the time of a single scan (Liu et al., 2017b). In this paradigm, the timing of CO2 and O2 inhalation were designed such that Et-CO2 and Et-O2 were modulated at different frequencies with a temporal correlation of close to zero. Then, the BOLD signal change to Et-CO2 change yields a CVR map, while the BOLD signal change to Et-O2 change yields a CBVv map. The time delay between physiological recordings and the BOLD signal yields a BAT map, and the residual BOLD signal can be analyzed to yield functional connectivity networks. This approach allows the measurement of multiple hemodynamic parameters within a clinically acceptable imaging time. Figure 7 shows four parametric maps obtained from this type of integrated vascular (iVas) MRI that employs concomitant CO2 and O2 challenges. It was found that all physiological maps derived from this method were of good quality and the image contrasts were comparable to current methods that require separate scans (Liu et al., 2017b).

In addition, with biophysical modeling of the BOLD signal, combined CO2 and O2 challenges can also be used to estimate baseline parameters for the oxygen consumption of the brain, including oxygen extraction fraction (OEF) and cerebral metabolic rate of oxygen (CMRO2) (Bulte et al., 2012; Gauthier et al., 2012; Merola et al., 2016; Wise et al., 2013).

9.2 CVR mapping without CO2 inhalation

CVR mapping with CO2 inhalation provides reliable results and has shown great promise in clinical applications (Chan et al., 2015; Fierstra et al., 2016; Han et al., 2008; Kenney et al., 2016; Mandell et al., 2008; Mikulis et al., 2005; Zhao et al., 2009). However, the requirement of inhaling a special gas mixture inside the MRI still presents a practical limitation to its application in clinical practice. There have been some efforts to perform CVR mapping without gas inhalation. These techniques include breath-hold, hyperventilation, and resting-state fMRI.

The breath-hold method induces hypercapnia by having the subjects hold their breath for a short period of time (usually 15–30 seconds), which leads to an increase in blood CO2 concentration (Bright and Murphy, 2013; Chan et al., 2015; de Boorder et al., 2004; Geranmayeh et al., 2015; Magon et al., 2009; Tancredi and Hoge, 2013; Zaca et al., 2014). In a breath-hold CVR experiment, MRI images are acquired during alternating periods of breath-holding and normal breathing (with a guided pace in some studies (Bright and Murphy, 2013; Tancredi and Hoge, 2013)). One difference between the breath-hold and CO2 inhalation is that, during the breath-hold period, CO2 concentration in the lung cannot be

measured, and thus, there is a gap in the CO_2 time course. Modeled stimulus time course (e.g., ramps and gamma-variate function) can be used to estimate CO_2 levels during this gap and applied as a regressor in the general linear model analysis. The advantage of the breath-hold CVR method is that no gas delivery system is required, which substantially simplifies the experimental procedure. A disadvantage is that this task requires considerable cooperation from the participant, which is particularly difficult for the elderly (Jahanian et al., 2017), and variations in adherence to the instruction can affect the data quality and reliability of this method (Magon et al., 2009). In contrast to the breath-hold method, which induces hypercapnia, hyperventilation that induces hypocapnia has also been used to measure CVR occasionally (Bright et al., 2009; Krainik et al., 2005). However, hyperventilation may lower Et-CO_2 to a level where the change in CBF is no longer linear to the change in Et-CO_2, resulting in underestimation of CVR (Bhogal et al., 2014; Tancredi and Hoge, 2013). For both breath-hold and hyperventilation tasks, subject motion is another potential concern. In addition, since breath-hold and hyperventilation could be considered motor tasks, the concomitant motor activation may affect the CVR estimation across the task-activated brain regions.

Recently, resting-state fMRI data, which are often acquired for functional connectivity mapping, have been shown to provide an estimation of CVR maps (Golestani et al., 2016; Jahanian et al., 2014; Liu et al., 2017a). Rather than manipulating the Et-CO_2 level by hypercapnia breathing or breath-holding, this approach utilizes spontaneous fluctuations in the breathing pattern, and thus the CO_2 level, to extract CVR information from the resting-state data. The BOLD signal fluctuations attributed to CO_2 variations can be extracted by either applying a temporal filtering (e.g., 0.02–0.04 Hz (Liu et al., 2017a) or <0.025 Hz (Jahanian et al., 2014)), or by factoring out other physiological signals from the resting state data (Golestani et al., 2015). Figure 8 shows two examples of CVR maps derived from resting-state BOLD data, one in a healthy volunteer and the other in a patient with cerebrovascular disease. Good agreement between resting-state CVR results and hypercapnia CVR results have been reported (Liu et al., 2017a). There have also been studies using the resting state fluctuation of amplitude (RSFA) and the amplitude of low-frequency fluctuation (ALFF) (Di et al., 2013; Kannurpatti and Biswal, 2008; Kannurpatti et al., 2014; Lipp et al., 2015; Tsvetanov et al., 2015) to approximate CVR. In general, the resting-state CVR method requires minimal subject compliance, and can be performed in patients with more severe conditions, such as acute stroke. A limitation of the resting-state methods is that, if the subject breathes regularly with minimal fluctuation in their Et-CO_2 level, there will not be enough CO_2-related signal variations for CVR evaluation. Nonetheless, CVR mapping with resting-state data has great potential in many clinical applications in which hypercapnia challenge is not feasible.

There are other methods to measure CVR, such as those that use an acetazolamide challenge together with single-photon emission computed tomography (SPECT) or transcranial Doppler ultrasound (TCD) (See (Settakis et al., 2003) for review). Those methods are beyond the scope of this review, which focuses on MRI techniques to measure CO_2-induced hemodynamic responses.

10. Conclusion

This work provides a technical review of an emerging technique to measure the brain's vascular reserve by evaluating cerebrovascular reactivity to CO2. We reviewed the physiological mechanisms and methodological aspects of this technique in terms of gas challenge, MRI acquisition, and data analysis. We also described alternative approaches for CVR mapping that do not require CO2 inhalation. MRI measurement of CVR is a promising technique in physiological imaging of the brain and has strong potential for a variety of basic science and clinical applications.

Acknowledgments

References

Ainsworth B, Marshall JE, Meron D, Baldwin DS, Chadwick P, Munafo MR, Garner M. 2015; Evaluating psychological interventions in a novel experimental human model of anxiety. J Psychiatr Res. 63:117–122. [PubMed: 25765144]

Askrog V. 1966; Changes in (a-A)CO2 difference and pulmonary artery pressure in anesthetized man. J Appl Physiol. 21:1299–1305. [PubMed: 5916666]

Aslan S, Xu F, Wang PL, Uh J, Yezhuvath US, van Osch M, Lu H. 2010; Estimation of labeling efficiency in pseudocontinuous arterial spin labeling. Magn Reson Med. 63:765–771. [PubMed: 20187183]

Bhavani-Shankar K, Kumar AY, Moseley HS, Ahyee-Hallsworth R. 1995; Terminology and the current limitations of time capnography: a brief review. J Clin Monit. 11:175–182. [PubMed: 7623057]

Bhogal AA, Philippens ME, Siero JC, Fisher JA, Petersen ET, Luijten PR, Hoogduin H. 2015; Examining the regional and cerebral depth-dependent BOLD cerebrovascular reactivity response at 7T. Neuroimage. 114:239–248. [PubMed: 25876215]

Bhogal AA, Siero JC, Fisher JA, Froeling M, Luijten P, Philippens M, Hoogduin H. 2014; Investigating the non-linearity of the BOLD cerebrovascular reactivity response to targeted hypo/hypercapnia at 7T. Neuroimage. 98:296–305. [PubMed: 24830840]

Blockley NP, Driver ID, Francis ST, Fisher JA, Gowland PA. 2011; An improved method for acquiring cerebrovascular reactivity maps. Magn Reson Med. 65:1278–1286. [PubMed: 21500256]

Blockley NP, Griffeth VE, Germuska MA, Bulte DP, Buxton RB. 2013; An analysis of the use of hyperoxia for measuring venous cerebral blood volume: comparison of the existing method with a new analysis approach. Neuroimage. 72:33–40. [PubMed: 23370053]

Blockley NP, Harkin JW, Bulte DP. 2017; Rapid cerebrovascular reactivity mapping: Enabling vascular reactivity information to be routinely acquired. Neuroimage. 159:214–223. [PubMed: 28756241]

Bolotina VM, Najibi S, Palacino JJ, Pagano PJ, Cohen RA. 1994; Nitric oxide directly activates calcium-dependent potassium channels in vascular smooth muscle. Nature. 368:850–853. [PubMed: 7512692]

Brayden JE. 1996; Potassium channels in vascular smooth muscle. Clin Exp Pharmacol Physiol. 23:1069–1076. [PubMed: 8977162]

Bright MG, Bulte DP, Jezzard P, Duyn JH. 2009; Characterization of regional heterogeneity in cerebrovascular reactivity dynamics using novel hypocapnia task and BOLD fMRI. Neuroimage. 48:166–175. [PubMed: 19450694]

Bright MG, Murphy K. 2013; Reliable quantification of BOLD fMRI cerebrovascular reactivity despite poor breath-hold performance. Neuroimage. 83:559–568. [PubMed: 23845426]

Bulte D, Chiarelli P, Wise R, Jezzard P. 2007; Measurement of cerebral blood volume in humans using hyperoxic MRI contrast. J Magn Reson Imaging. 26:894–899. [PubMed: 17896390]

Bulte DP, Drescher K, Jezzard P. 2009; Comparison of hypercapnia-based calibration techniques for measurement of cerebral oxygen metabolism with MRI. Magn Reson Med. 61:391–398. [PubMed: 19165902]

Bulte DP, Kelly M, Germuska M, Xie J, Chappell MA, Okell TW, Bright MG, Jezzard P. 2012; Quantitative measurement of cerebral physiology using respiratory-calibrated MRI. Neuroimage. 60:582–591. [PubMed: 22209811]

Burrows MDFRCPC, Frederick A. 1989; Physiologic Dead Space, Venous Admixture, and the Arterial to End-tidal Carbon Dioxide Difference in Infants and Children Undergoing Cardiac Surgery. Anesthesiology. 70:219–225. [PubMed: 2492409]

Caputi L, Ghielmetti F, Farago G, Longaretti F, Lamperti M, Anzola GP, Carriero MR, Charbel FT, Bruzzone MG, Parati E, Ciceri E. 2014; Cerebrovascular reactivity by quantitative magnetic resonance angiography with a Co(2) challenge. Validation as a new imaging biomarker. Eur J Radiol. 83:1005–1010. [PubMed: 24721002]

Chan ST, Evans KC, Rosen BR, Song TY, Kwong KK. 2015; A case study of magnetic resonance imaging of cerebrovascular reactivity: a powerful imaging marker for mild traumatic brain injury. Brain Inj. 29:403–407. [PubMed: 25384127]

Chen JJ, Pike GB. 2010; Global cerebral oxidative metabolism during hypercapnia and hypocapnia in humans: implications for BOLD fMRI. J Cereb Blood Flow Metab. 30:1094–1099. [PubMed: 20372169]

Chen Y, Wang DJ, Detre JA. 2011; Test-retest reliability of arterial spin labeling with common labeling strategies. J Magn Reson Imaging. 33:940–949. [PubMed: 21448961]

Christen T, Jahanian H, Ni WW, Qiu D, Moseley ME, Zaharchuk G. 2015; Noncontrast mapping of arterial delay and functional connectivity using resting-state functional MRI: a study in Moyamoya patients. J Magn Reson Imaging. 41:424–430. [PubMed: 24419985]

Davis TL, Kwong KK, Weisskoff RM, Rosen BR. 1998; Calibrated functional MRI: mapping the dynamics of oxidative metabolism. Proc Natl Acad Sci U S A. 95:1834–1839. [PubMed: 9465103]

de Boorder MJ, Hendrikse J, van der Grond J. 2004; Phase-contrast magnetic resonance imaging measurements of cerebral autoregulation with a breath-hold challenge: a feasibility study. Stroke. 35:1350–1354. [PubMed: 15131315]

De Vis JB, Hendrikse J, Bhogal A, Adams A, Kappelle LJ, Petersen ET. 2015a; Age-related changes in brain hemodynamics; A calibrated MRI study. Hum Brain Mapp. 36:3973–3987. [PubMed: 26177724]

De Vis JB, Petersen ET, Bhogal A, Hartkamp NS, Klijn CJ, Kappelle LJ, Hendrikse J. 2015b; Calibrated MRI to evaluate cerebral hemodynamics in patients with an internal carotid artery occlusion. J Cereb Blood Flow Metab. 35:1015–1023. [PubMed: 25712500]

Di X, Kannurpatti SS, Rypma B, Biswal BB. 2013; Calibrating BOLD fMRI activations with neurovascular and anatomical constraints. Cereb Cortex. 23:255–263. [PubMed: 22345358]

Donahue MJ, Ayad M, Moore R, van Osch M, Singer R, Clemmons P, Strother M. 2013; Relationships between hypercarbic reactivity, cerebral blood flow, and arterial circulation times in patients with moyamoya disease. J Magn Reson Imaging. doi: 10.1002/jmri.24070

Donahue MJ, Dethrage LM, Faraco CC, Jordan LC, Clemmons P, Singer R, Mocco J, Shyr Y, Desai A, O'Duffy A, Riebau D, Hermann L, Connors J, Kirshner H, Strother MK. 2014a; Routine Clinical Evaluation of Cerebrovascular Reserve Capacity Using Carbogen in Patients With Intracranial Stenosis. Stroke. 45:2335–2341. [PubMed: 24938845]

Donahue MJ, Faraco CC, Strother MK, Chappell MA, Rane S, Dethrage LM, Hendrikse J, Siero JC. 2014b; Bolus arrival time and cerebral blood flow responses to hypercarbia. J Cereb Blood Flow Metab. 34:1243–1252. [PubMed: 24780904]

Donahue MJ, Strother MK, Lindsey KP, Hocke LM, Tong Y, Frederick BD. 2016; Time delay processing of hypercapnic fMRI allows quantitative parameterization of cerebrovascular reactivity and blood flow delays. J Cereb Blood Flow Metab. 36:1767–1779. [PubMed: 26661192]

Driver I, Blockley N, Fisher J, Francis S, Gowland P. 2010; The change in cerebrovascular reactivity between 3 T and 7 T measured using graded hypercapnia. Neuroimage. 51:274–279. [PubMed: 20056163]

Driver ID, Whittaker JR, Bright MG, Muthukumaraswamy SD, Murphy K. 2016; Arterial CO2 Fluctuations Modulate Neuronal Rhythmicity: Implications for MEG and fMRI Studies of Resting-State Networks. J Neurosci. 36:8541–8550. [PubMed: 27535903]

Duffin J, Sobczyk O, Crawley AP, Poublanc J, Mikulis DJ, Fisher JA. 2015; The dynamics of cerebrovascular reactivity shown with transfer function analysis. Neuroimage. 114:207–216. [PubMed: 25891374]

Fathi AR, Yang C, Bakhtian KD, Qi M, Lonser RR, Pluta RM. 2011; Carbon dioxide influence on nitric oxide production in endothelial cells and astrocytes: cellular mechanisms. Brain Res. 1386:50–57. [PubMed: 21362408]

Fierstra J, Sobczyk O, Battisti-Charbonney A, Mandell DM, Poublanc J, Crawley AP, Mikulis DJ, Duffin J, Fisher JA. 2013; Measuring cerebrovascular reactivity: what stimulus to use? J Physiol. 591:5809–5821. [PubMed: 24081155]

Fierstra J, van Niftrik B, Piccirelli M, Burkhardt JK, Pangalu A, Kocian R, Valavanis A, Weller M, Regli L, Bozinov O. 2016; Altered intraoperative cerebrovascular reactivity in brain areas of high-grade glioma recurrence. Magn Reson Imaging. 34:803–808. [PubMed: 26968146]

Fisher JA, Sobczyk O, Crawley A, Poublanc J, Dufort P, Venkatraghavan L, Sam K, Mikulis D, Duffin J. 2017 Assessing cerebrovascular reactivity by the pattern of response to progressive hypercapnia. Hum Brain Mapp.

Fletcher R, Jonson B, Cumming G, Brew J. 1981; THE CONCEPT OF DEADSPACE WITH SPECIAL REFERENCE TO THE SINGLE BREATH TEST FOR CARBON DIOXIDE. British Journal of Anaesthesia. 53:77–88. [PubMed: 6779846]

Fujishima M, Scheinberg P, Busto R, Reinmuth OM. 1971; The relation between cerebral oxygen consumption and cerebral vascular reactivity to carbon dioxide. Stroke. 2:251–257. [PubMed: 5111573]

Gauthier CJ, Desjardins-Crepeau L, Madjar C, Bherer L, Hoge RD. 2012; Absolute quantification of resting oxygen metabolism and metabolic reactivity during functional activation using QUO2 MRI. Neuroimage. 63:1353–1363. [PubMed: 22986357]

Gauthier CJ, Lefort M, Mekary S, Desjardins-Crepeau L, Skimminge A, Iversen P, Madjar C, Desjardins M, Lesage F, Garde E, Frouin F, Bherer L, Hoge RD. 2015; Hearts and minds: linking vascular rigidity and aerobic fitness with cognitive aging. Neurobiol Aging. 36:304–314. [PubMed: 25308963]

Gauthier CJ, Madjar C, Desjardins-Crepeau L, Bellec P, Bherer L, Hoge RD. 2013; Age dependence of hemodynamic response characteristics in human functional magnetic resonance imaging. Neurobiol Aging. 34:1469–1485. [PubMed: 23218565]

Geranmayeh F, Wise RJ, Leech R, Murphy K. 2015; Measuring vascular reactivity with breath-holds after stroke: a method to aid interpretation of group-level BOLD signal changes in longitudinal fMRI studies. Hum Brain Mapp. 36:1755–1771. [PubMed: 25727648]

Golestani AM, Chang C, Kwinta JB, Khatamian YB, Jean Chen J. 2015; Mapping the end-tidal CO2 response function in the resting-state BOLD fMRI signal: spatial specificity, test-retest reliability and effect of fMRI sampling rate. Neuroimage. 104:266–277. [PubMed: 25462695]

Golestani AM, Wei LL, Chen JJ. 2016; Quantitative mapping of cerebrovascular reactivity using resting-state BOLD fMRI: Validation in healthy adults. Neuroimage. 138:147–163. [PubMed: 27177763]

Greenberg SM. 2006; Small vessels, big problems. N Engl J Med. 354:1451–1453. [PubMed: 16598043]

Gupta A, Chazen JL, Hartman M, Delgado D, Anumula N, Shao H, Mazumdar M, Segal AZ, Kamel H, Leifer D, Sanelli PC. 2012; Cerebrovascular reserve and stroke risk in patients with carotid stenosis or occlusion: a systematic review and meta-analysis. Stroke. 43:2884–2891. [PubMed: 23091119]

Halani S, Kwinta JB, Golestani AM, Khatamian YB, Chen JJ. 2015; Comparing cerebrovascular reactivity measured using BOLD and cerebral blood flow MRI: The effect of basal vascular tension on vasodilatory and vasoconstrictive reactivity. Neuroimage. 110:110–123. [PubMed: 25655446]

Han JS, Mandell DM, Poublanc J, Mardimae A, Slessarev M, Jaigobin C, Fisher JA, Mikulis DJ. 2008; BOLD-MRI cerebrovascular reactivity findings in cocaine-induced cerebral vasculitis. Nat Clin Pract Neurol. 4:628–632. [PubMed: 18839005]

Hare HV, Germuska M, Kelly ME, Bulte DP. 2013; Comparison of CO2 in air versus carbogen for the measurement of cerebrovascular reactivity with magnetic resonance imaging. J Cereb Blood Flow Metab. 33:1799–1805. [PubMed: 23921896]

Heijtel DF, Mutsaerts HJ, Bakker E, Schober P, Stevens MF, Petersen ET, van Berckel BN, Majoie CB, Booij J, van Osch MJ, Vanbavel E, Boellaard R, Lammertsma AA, Nederveen AJ. 2014; Accuracy and precision of pseudo-continuous arterial spin labeling perfusion during baseline and hypercapnia: a head-to-head comparison with (1)(5)O H(2)O positron emission tomography. Neuroimage. 92:182–192. [PubMed: 24531046]

Ho YC, Petersen ET, Zimine I, Golay X. 2011; Similarities and differences in arterial responses to hypercapnia and visual stimulation. J Cereb Blood Flow Metab. 31:560–571. [PubMed: 20700127]

Hoge RD, Atkinson J, Gill B, Crelier GR, Marrett S, Pike GB. 1999; Investigation of BOLD signal dependence on cerebral blood flow and oxygen consumption: the deoxyhemoglobin dilution model. Magn Reson Med. 42:849–863. [PubMed: 10542343]

Hou, X, Liu, P, Chan, M, Wig, G, Park, DC, Lu, H. On the feasibility of estimating functional connectivity from hypercapnia BOLD MRI data. Proceedings of ISMRM 25rd Annual Meeting; Honolulu, HI, USA: 2017. 5371

Jahanian H, Christen T, Moseley ME, Pajewski NM, Wright CB, Tamura MK, Zaharchuk G, Group SSR. 2017; Measuring vascular reactivity with resting-state blood oxygenation level-dependent (BOLD) signal fluctuations: A potential alternative to the breath-holding challenge? J Cereb Blood Flow Metab. 37:2526–2538. [PubMed: 27683452]

Jahanian H, Ni WW, Christen T, Moseley ME, Kurella Tamura M, Zaharchuk G. 2014; Spontaneous BOLD signal fluctuations in young healthy subjects and elderly patients with chronic kidney disease. PLoS One. 9:e92539. [PubMed: 24651703]

Jain V, Langham MC, Floyd TF, Jain G, Magland JF, Wehrli FW. 2011; Rapid magnetic resonance measurement of global cerebral metabolic rate of oxygen consumption in humans during rest and hypercapnia. J Cereb Blood Flow Metab. 31:1504–1512. [PubMed: 21505481]

Kannurpatti SS, Biswal BB. 2008; Detection and scaling of task-induced fMRI-BOLD response using resting state fluctuations. Neuroimage. 40:1567–1574. [PubMed: 18343159]

Kannurpatti SS, Motes MA, Biswal BB, Rypma B. 2014; Assessment of unconstrained cerebrovascular reactivity marker for large age-range FMRI studies. PLoS One. 9:e88751. [PubMed: 24551151]

Kassner A, Winter JD, Poublanc J, Mikulis DJ, Crawley AP. 2010; Blood-oxygen level dependent MRI measures of cerebrovascular reactivity using a controlled respiratory challenge: reproducibility and gender differences. J Magn Reson Imaging. 31:298–304. [PubMed: 20099341]

Kenney K, Amyot F, Haber M, Pronger A, Bogoslovsky T, Moore C, Diaz-Arrastia R. 2016; Cerebral Vascular Injury in Traumatic Brain Injury. Exp Neurol 275 Pt. 3:353–366.

Krainik A, Hund-Georgiadis M, Zysset S, von Cramon DY. 2005; Regional impairment of cerebrovascular reactivity and BOLD signal in adults after stroke. Stroke. 36:1146–1152. [PubMed: 15879326]

Lajoie I, Tancredi FB, Hoge RD. 2016; Regional Reproducibility of BOLD Calibration Parameter M, OEF and Resting-State CMRO2 Measurements with QUO2 MRI. PLoS One. 11:e0163071. [PubMed: 27649493]

Leoni RF, Oliveira IA, Pontes-Neto OM, Santos AC, Leite JP. 2017; Cerebral blood flow and vasoreactivity in aging: an arterial spin labeling study. Braz J Med Biol Res. 50:e5670. [PubMed: 28355354]

Leung J, Behpour A, Sokol N, Mohanta A, Kassner A. 2013; Assessment of intracranial blood flow velocities using a computer controlled vasoactive stimulus: a comparison between phase contrast magnetic resonance angiography and transcranial Doppler ultrasonography. J Magn Reson Imaging. 38:733–738. [PubMed: 23148038]

Lipp I, Murphy K, Caseras X, Wise RG. 2015; Agreement and repeatability of vascular reactivity estimates based on a breath-hold task and a resting state scan. Neuroimage. 113:387–396. [PubMed: 25795342]

Liu P, Hebrank AC, Rodrigue KM, Kennedy KM, Park DC, Lu H. 2013a; A comparison of physiologic modulators of fMRI signals. Hum Brain Mapp. 34:2078–2088. [PubMed: 22461234]

Liu P, Hebrank AC, Rodrigue KM, Kennedy KM, Section J, Park DC, Lu H. 2013b; Age-related differences in memory-encoding fMRI responses after accounting for decline in vascular reactivity. Neuroimage. 78:415–425. [PubMed: 23624491]

Liu P, Li Y, Pinho M, Park DC, Welch BG, Lu H. 2017a; Cerebrovascular reactivity mapping without gas challenges. Neuroimage. 146:320–326. [PubMed: 27888058]

Liu P, Welch BG, Li Y, Gu H, King D, Yang Y, Pinho M, Lu H. 2017b; Multiparametric imaging of brain hemodynamics and function using gas-inhalation MRI. Neuroimage. 146:715–723. [PubMed: 27693197]

Liu P, Xu F, Lu H. 2013c; Test-retest reproducibility of a rapid method to measure brain oxygen metabolism. Magn Reson Med. 69:675–681. [PubMed: 22517498]

Liu YJ, Huang TY, Lee YH, Juan CJ. 2012; The cerebral vasomotor response in varying CO(2) concentrations, as evaluated using cine phase contrast MRI: Flow, volume, and cerebrovascular resistance indices. Med Phys. 39:6534–6541. [PubMed: 23127048]

Lu H, Liu P, Yezhuvath U, Cheng Y, Marshall O, Ge Y. 2014MRI mapping of cerebrovascular reactivity via gas inhalation challenges. J Vis Exp.

Lu H, Xu F, Rodrigue KM, Kennedy KM, Cheng Y, Flicker B, Hebrank AC, Uh J, Park DC. 2011; Alterations in cerebral metabolic rate and blood supply across the adult lifespan. Cereb Cortex. 21:1426–1434. [PubMed: 21051551]

Magon S, Basso G, Farace P, Ricciardi GK, Beltramello A, Sbarbati A. 2009; Reproducibility of BOLD signal change induced by breath holding. Neuroimage. 45:702–712. [PubMed: 19211035]

Mandell DM, Han JS, Poublanc J, Crawley AP, Stainsby JA, Fisher JA, Mikulis DJ. 2008; Mapping cerebrovascular reactivity using blood oxygen level-dependent MRI in Patients with arterial steno-occlusive disease: comparison with arterial spin labeling MRI. Stroke. 39:2021–2028. [PubMed: 18451352]

Mark CI, Slessarev M, Ito S, Han J, Fisher JA, Pike GB. 2010; Precise control of end-tidal carbon dioxide and oxygen improves BOLD and ASL cerebrovascular reactivity measures. Magn Reson Med. 64:749–756. [PubMed: 20648687]

Marstrand JR, Garde E, Rostrup E, Ring P, Rosenbaum S, Mortensen EL, Larsson HB. 2002; Cerebral perfusion and cerebrovascular reactivity are reduced in white matter hyperintensities. Stroke. 33:972–976. [PubMed: 11935046]

McSwain SD, Hamel DS, Smith PB, Gentile MA, Srinivasan S, Meliones JN, Cheifetz IM. 2010; End-tidal and arterial carbon dioxide measurements correlate across all levels of physiologic dead space. Respir Care. 55:288–293. [PubMed: 20196877]

Merola A, Germuska MA, Warnert EA, Richmond L, Helme D, Khot S, Murphy K, Rogers PJ, Hall JE, Wise RG. 2017; Mapping the pharmacological modulation of brain oxygen metabolism: The effects of caffeine on absolute CMRO2 measured using dual calibrated fMRI. Neuroimage. 155:331–343. [PubMed: 28323164]

Merola A, Murphy K, Stone AJ, Germuska MA, Griffeth VEM, Blockley NP, Buxton RB, Wise RG. 2016; Measurement of oxygen extraction fraction (OEF): An optimized BOLD signal model for use with hypercapnic and hyperoxic calibration. Neuroimage. 129:159–174. [PubMed: 26801605]

Mikulis DJ, Krolczyk G, Desal H, Logan W, Deveber G, Dirks P, Tymianski M, Crawley A, Vesely A, Kassner A, Preiss D, Somogyi R, Fisher JA. 2005; Preoperative and postoperative mapping of cerebrovascular reactivity in moyamoya disease by using blood oxygen level-dependent magnetic resonance imaging. J Neurosurg. 103:347–355. [PubMed: 16175867]

Moreton FC, Dani KA, Goutcher C, O'Hare K, Muir KW. 2016; Respiratory challenge MRI: Practical aspects. NeuroImage: Clinical. 11:667–677. [PubMed: 27330967]

Nunn JF, Hill DW. 1960; Respiratory dead space and arterial to end-tidal carbon dioxide tension difference in anesthetized man. J Appl Physiol. 15:383–389. [PubMed: 14427915]

Oudegeest-Sander MH, van Beek AH, Abbink K, Olde Rikkert MG, Hopman MT, Claassen JA. 2014; Assessment of dynamic cerebral autoregulation and cerebrovascular CO2 reactivity in ageing by measurements of cerebral blood flow and cortical oxygenation. Exp Physiol. 99:586–598. [PubMed: 24363382]

Peebles K, Celi L, McGrattan K, Murrell C, Thomas K, Ainslie PN. 2007; Human cerebrovascular and ventilatory CO2 reactivity to end-tidal, arterial and internal jugular vein PCO2. J Physiol. 584:347–357. [PubMed: 17690148]

Peng HL, Jensen PE, Nilsson H, Aalkjaer C. 1998; Effect of acidosis on tension and [Ca2+]i in rat cerebral arteries: is there a role for membrane potential? Am J Physiol. 274:H655–662. [PubMed: 9486271]

Pillai JJ, Zaca D. 2011; Clinical utility of cerebrovascular reactivity mapping in patients with low grade gliomas. World J Clin Oncol. 2:397–403. [PubMed: 22171282]

Poublanc J, Crawley AP, Sobczyk O, Montandon G, Sam K, Mandell DM, Dufort P, Venkatraghavan L, Duffin J, Mikulis DJ, Fisher JA. 2015; Measuring cerebrovascular reactivity: the dynamic response to a step hypercapnic stimulus. J Cereb Blood Flow Metab. 35:1746–1756. [PubMed: 26126862]

Ravi H, Liu P, Peng SL, Liu H, Lu H. 2016a; Simultaneous multi-slice (SMS) acquisition enhances the sensitivity of hemodynamic mapping using gas challenges. NMR Biomed. 29:1511–1518. [PubMed: 27598821]

Ravi H, Thomas BP, Peng SL, Liu H, Lu H. 2016b; On the optimization of imaging protocol for the mapping of cerebrovascular reactivity. J Magn Reson Imaging. 43:661–668. [PubMed: 26268541]

Restom K, Perthen JE, Liu TT. 2008; Calibrated fMRI in the medial temporal lobe during a memory-encoding task. Neuroimage. 40:1495–1502. [PubMed: 18329291]

Rostrup E, Law I, Blinkenberg M, Larsson HB, Born AP, Holm S, Paulson OB. 2000; Regional differences in the CBF and BOLD responses to hypercapnia: a combined PET and fMRI study. Neuroimage. 11:87–97. [PubMed: 10679182]

Sandow SL, Haddock RE, Hill CE, Chadha PS, Kerr PM, Welsh DG, Plane F. 2009; What's where and why at a vascular myoendothelial microdomain signalling complex. Clin Exp Pharmacol Physiol. 36:67–76. [PubMed: 19018806]

Settakis G, Molnar C, Kerenyi L, Kollar J, Legemate D, Csiba L, Fulesdi B. 2003; Acetazolamide as a vasodilatory stimulus in cerebrovascular diseases and in conditions affecting the cerebral vasculature. Eur J Neurol. 10:609–620. [PubMed: 14641504]

Slessarev M, Han J, Mardimae A, Prisman E, Preiss D, Volgyesi G, Ansel C, Duffin J, Fisher JA. 2007; Prospective targeting and control of end-tidal CO2 and O2 concentrations. J Physiol. 581:1207–1219. [PubMed: 17446225]

Sobczyk O, Battisti-Charbonney A, Fierstra J, Mandell DM, Poublanc J, Crawley AP, Mikulis DJ, Duffin J, Fisher JA. 2014; A conceptual model for CO(2)-induced redistribution of cerebral blood flow with experimental confirmation using BOLD MRI. Neuroimage. 92:56–68. [PubMed: 24508647]

Song Z, McDonough IM, Liu P, Lu H, Park DC. 2016; Cortical amyloid burden and age moderate hippocampal activity in cognitively-normal adults. Neuroimage Clin. 12:78–84. [PubMed: 27408792]

Spano VR, Mandell DM, Poublanc J, Sam K, Battisti-Charbonney A, Pucci O, Han JS, Crawley AP, Fisher JA, Mikulis DJ. 2013; CO2 blood oxygen level-dependent MR mapping of cerebrovascular reserve in a clinical population: safety, tolerability, and technical feasibility. Radiology. 266:592–598. [PubMed: 23204541]

Su P, Mao D, Liu P, Li Y, Pinho MC, Welch BG, Lu H. 2017; Multiparametric estimation of brain hemodynamics with MR fingerprinting ASL. Magn Reson Med. 78:1812–1823. [PubMed: 28019021]

Sullivan KJ, Kissoon N, Goodwin SR. 2005; End-tidal carbon dioxide monitoring in pediatric emergencies. Pediatr Emerg Care. 21:327–332. [PubMed: 15874818]

Tancredi FB, Girouard H, Hoge RD. 2015; Modeling the role of osmotic forces in the cerebrovascular response to CO2. Med Hypotheses. 85:25–36. [PubMed: 25858437]

Tancredi FB, Hoge RD. 2013; Comparison of cerebral vascular reactivity measures obtained using breath-holding and CO2 inhalation. J Cereb Blood Flow Metab. 33:1066–1074. [PubMed: 23571282]

Tancredi FB, Lajoie I, Hoge RD. 2014; A simple breathing circuit allowing precise control of inspiratory gases for experimental respiratory manipulations. BMC Res Notes. 7:235. [PubMed: 24725848]

Tchistiakova E, Anderson ND, Greenwood CE, MacIntosh BJ. 2014; Combined effects of type 2 diabetes and hypertension associated with cortical thinning and impaired cerebrovascular reactivity relative to hypertension alone in older adults. Neuroimage Clin. 5:36–41. [PubMed: 24967157]

Thomas BP, Liu P, Aslan S, King KS, van Osch MJ, Lu H. 2013; Physiologic underpinnings of negative BOLD cerebrovascular reactivity in brain ventricles. Neuroimage. 83:505–512. [PubMed: 23851322]

Thomas BP, Liu P, Park DC, van Osch MJ, Lu H. 2014; Cerebrovascular reactivity in the brain white matter: magnitude, temporal characteristics, and age effects. J Cereb Blood Flow Metab. 34:242–247. [PubMed: 24192640]

Tong Y, Bergethon PR, Frederick BD. 2011; An improved method for mapping cerebrovascular reserve using concurrent fMRI and near-infrared spectroscopy with Regressor Interpolation at Progressive Time Delays (RIPTiDe). Neuroimage. 56:2047–2057. [PubMed: 21459147]

Tsvetanov KA, Henson RN, Tyler LK, Davis SW, Shafto MA, Taylor JR, Williams N, Cam C, Rowe JB. 2015; The effect of ageing on fMRI: Correction for the confounding effects of vascular reactivity evaluated by joint fMRI and MEG in 335 adults. Hum Brain Mapp. 36:2248–2269. [PubMed: 25727740]

Whittaker JR, Driver ID, Bright MG, Murphy K. 2016; The absolute CBF response to activation is preserved during elevated perfusion: Implications for neurovascular coupling measures. Neuroimage. 125:198–207. [PubMed: 26477657]

Williams EM, Hamilton RM, Sutton L, Viale JP, Hahn CE. 1997; Alveolar and dead space volume measured by oscillations of inspired oxygen in awake adults. Am J Respir Crit Care Med. 156:1834–1839. [PubMed: 9412563]

Wise RG, Harris AD, Stone AJ, Murphy K. 2013; Measurement of OEF and absolute CMRO2: MRI-based methods using interleaved and combined hypercapnia and hyperoxia. Neuroimage. 83:135–147. [PubMed: 23769703]

Wise RG, Pattinson KT, Bulte DP, Chiarelli PA, Mayhew SD, Balanos GM, O'Connor DF, Pragnell TR, Robbins PA, Tracey I, Jezzard P. 2007; Dynamic forcing of end-tidal carbon dioxide and oxygen applied to functional magnetic resonance imaging. J Cereb Blood Flow Metab. 27:1521–1532. [PubMed: 17406659]

Xu F, Uh J, Brier MR, Hart J Jr, Yezhuvath US, Gu H, Yang Y, Lu H. 2011; The influence of carbon dioxide on brain activity and metabolism in conscious humans. J Cereb Blood Flow Metab. 31:58–67. [PubMed: 20842164]

Xu HL, Koenig HM, Ye S, Feinstein DL, Pelligrino DA. 2004; Influence of the glia limitans on pial arteriolar relaxation in the rat. Am J Physiol Heart Circ Physiol. 287:H331–339. [PubMed: 14962837]

Yamanaka MK, Sue DY. 1987; Comparison of arterial-end-tidal PCO2 difference and dead space/tidal volume ratio in respiratory failure. Chest. 92:832–835. [PubMed: 3117500]

Yezhuvath US, Lewis-Amezcua K, Varghese R, Xiao G, Lu H. 2009; On the assessment of cerebrovascular reactivity using hypercapnia BOLD MRI. NMR Biomed. 22:779–786. [PubMed: 19388006]

Yoon SH, Zuccarello M, Rapoport RM. 2000; Reversal of hypercapnia induces endothelin-dependent constriction of basilar artery in rabbits with acute metabolic alkalosis. Gen Pharmacol. 35:333–340. [PubMed: 11922964]

Zaca D, Jovicich J, Nadar SR, Voyvodic JT, Pillai JJ. 2014; Cerebrovascular reactivity mapping in patients with low grade gliomas undergoing presurgical sensorimotor mapping with BOLD fMRI. J Magn Reson Imaging. 40:383–390. [PubMed: 24338845]

Zhao P, Alsop DC, Abduljalil A, Selim M, Lipsitz L, Novak P, Caplan L, Hu K, Novak V. 2009; Vasoreactivity and peri-infarct hyperintensities in stroke. Neurology. 72:643–649. [PubMed: 19221298]

Zhao Y, Vanhoutte PM, Leung SW. 2015; Vascular nitric oxide: Beyond eNOS. J Pharmacol Sci. 129:83–94. [PubMed: 26499181]

Ziegelstein RC, Cheng L, Blank PS, Spurgeon HA, Lakatta EG, Hansford RG, Capogrossi MC. 1993; Modulation of calcium homeostasis in cultured rat aortic endothelial cells by intracellular acidification. Am J Physiol. 265:H1424–1433. [PubMed: 8238429]
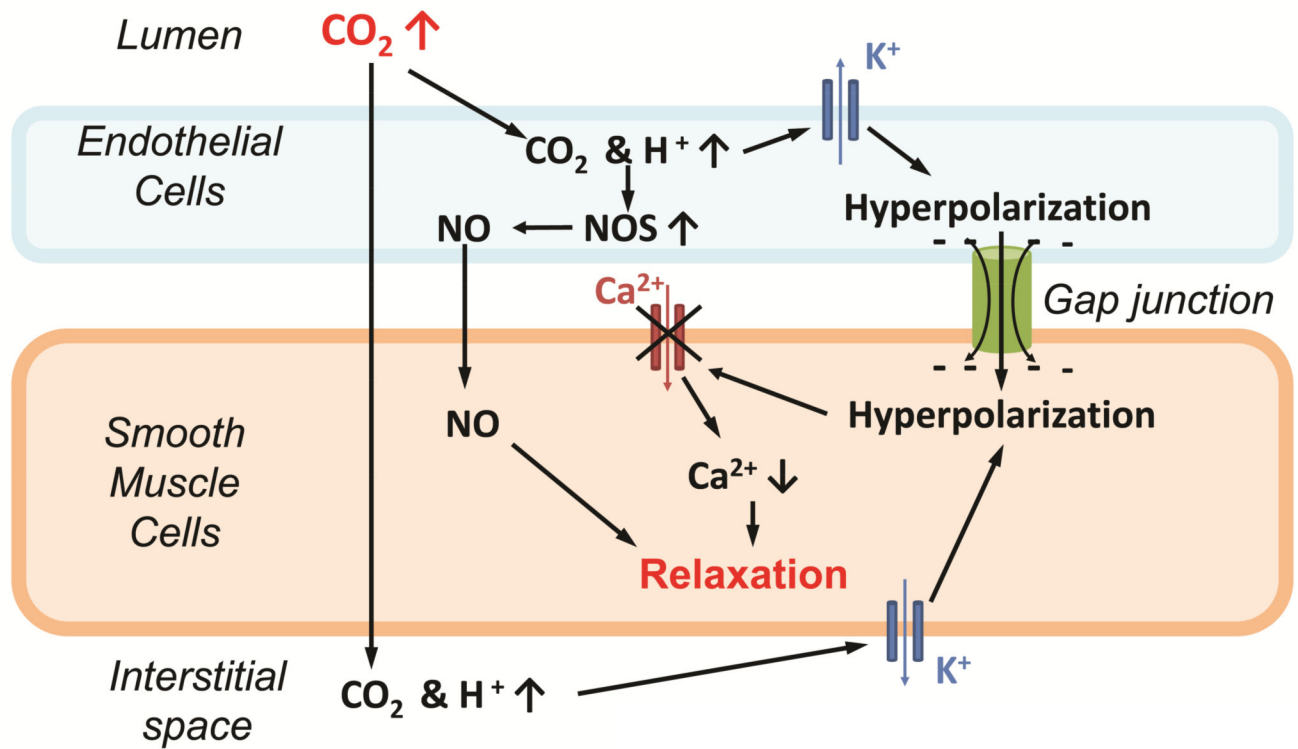
Figure 1.
Mechanisms of vessel dilation as a result of CO2 inhalation. CO2 and the associated increase in H^+ can cause hyperpolarization of smooth muscle cells directly or indirectly via endothelial cells.
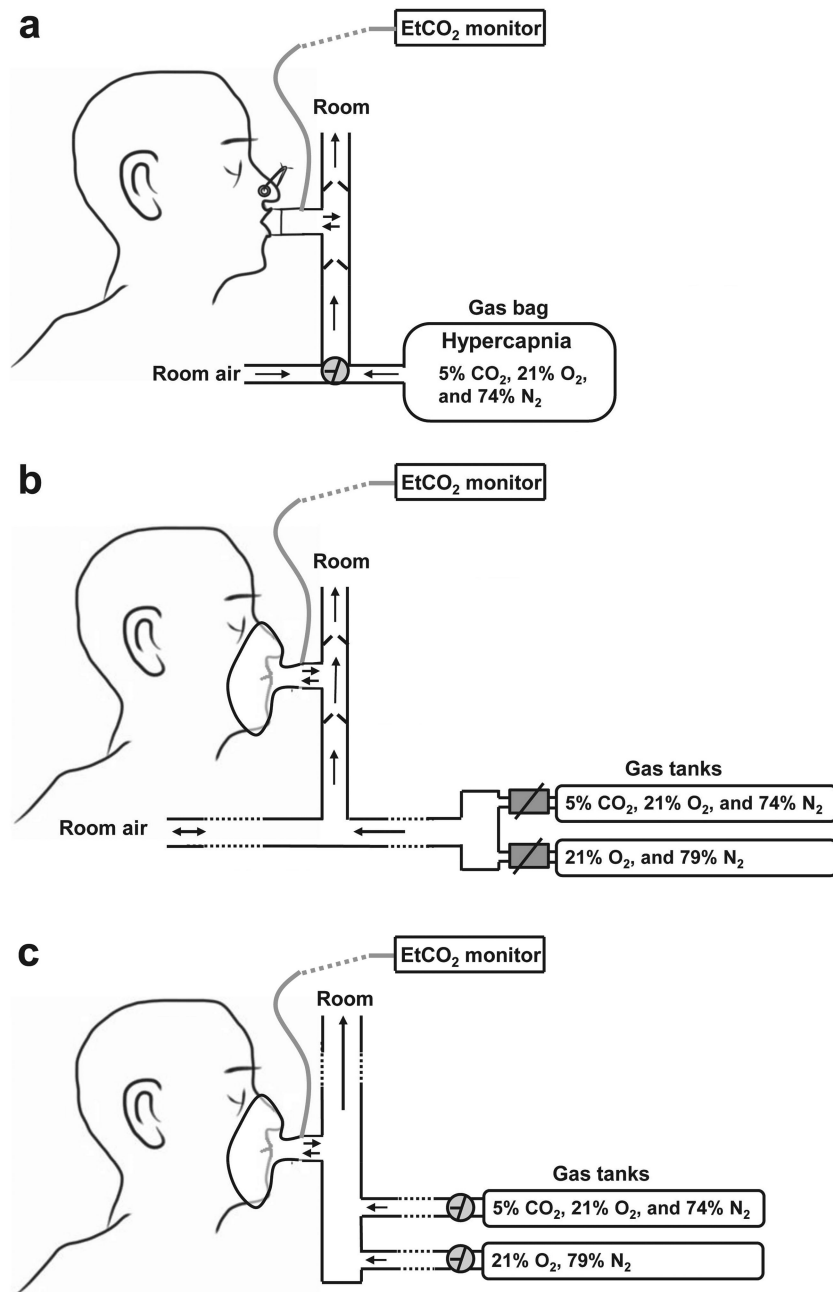
Figure 2.
Three systems of gas delivery apparatus with a fixed CO2 concentration in inspired air. (a) Breathing apparatus by Lu et al. (b) Breathing apparatus by Tancredi et al. (c) Breathing apparatus by Bulte et al.
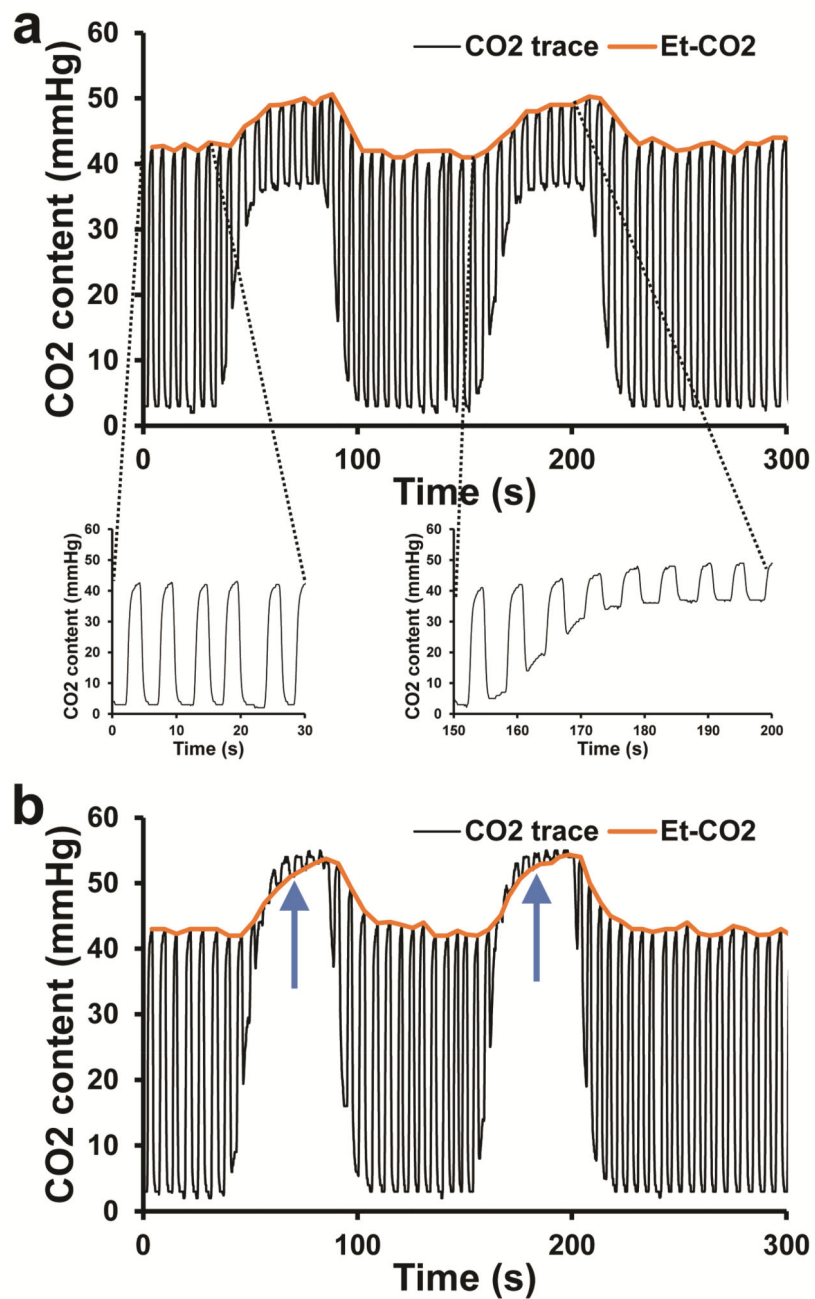
Figure 3.
Example of CO2 time course during the experiment. (a) CO2 time course with 5% CO2 inhalation. Segments of the breath-by-breath CO2 content trace, as recorded by the CO2 monitor, are shown for a room-air breathing period (left inset) and a 5% CO2 inhalation period (right inset). (b) CO2 time course with 7.5% CO2 inhalation. Blue arrows indicate the periods where the inhaled CO2 concentration exceeded the exhaled CO2 concentration. Extracted Et-CO2 time courses are shown by the orange curve.
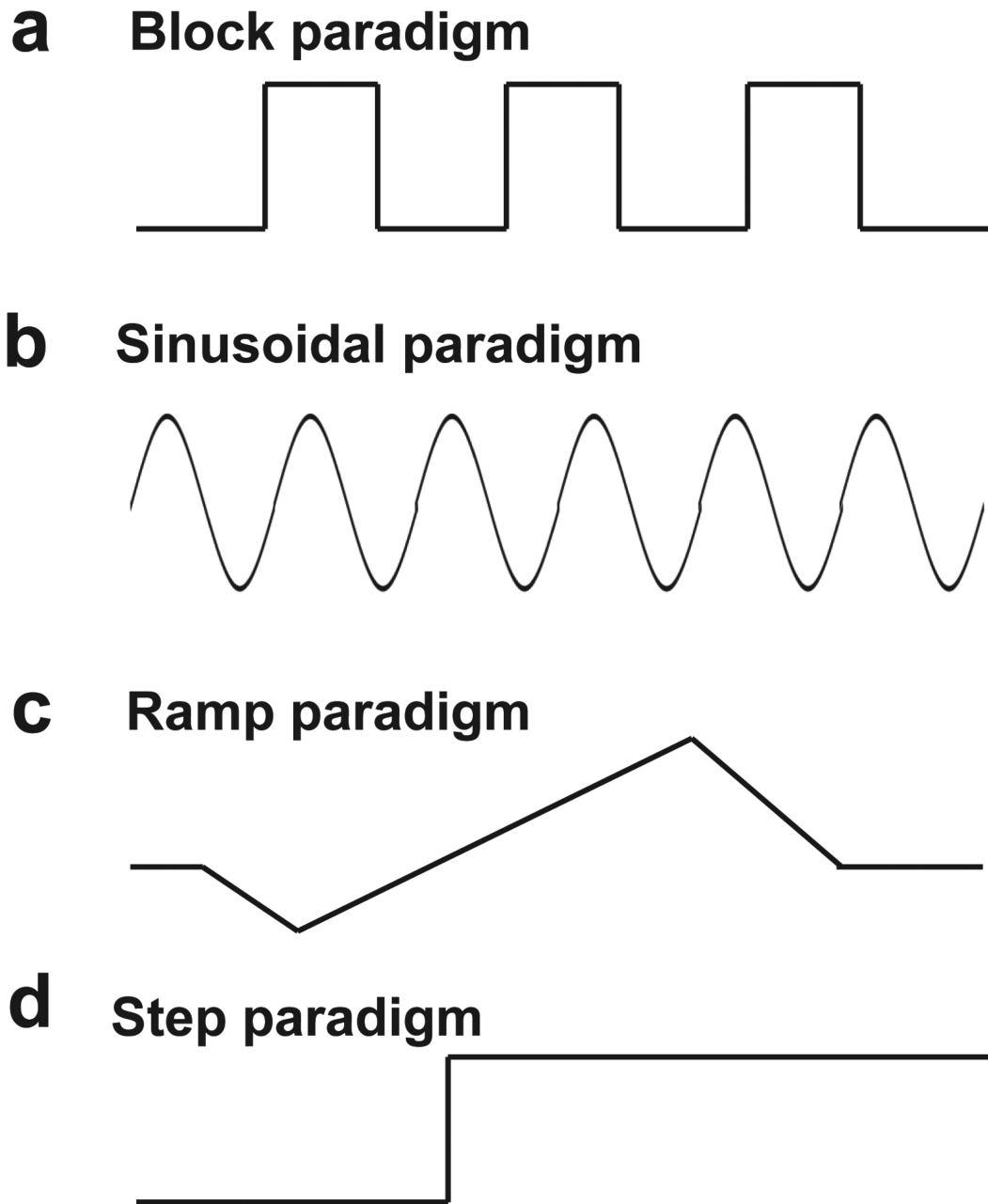
a **Block paradigm**

b **Sinusoidal paradigm**

c **Ramp paradigm**

d **Step paradigm**

Figure 4.
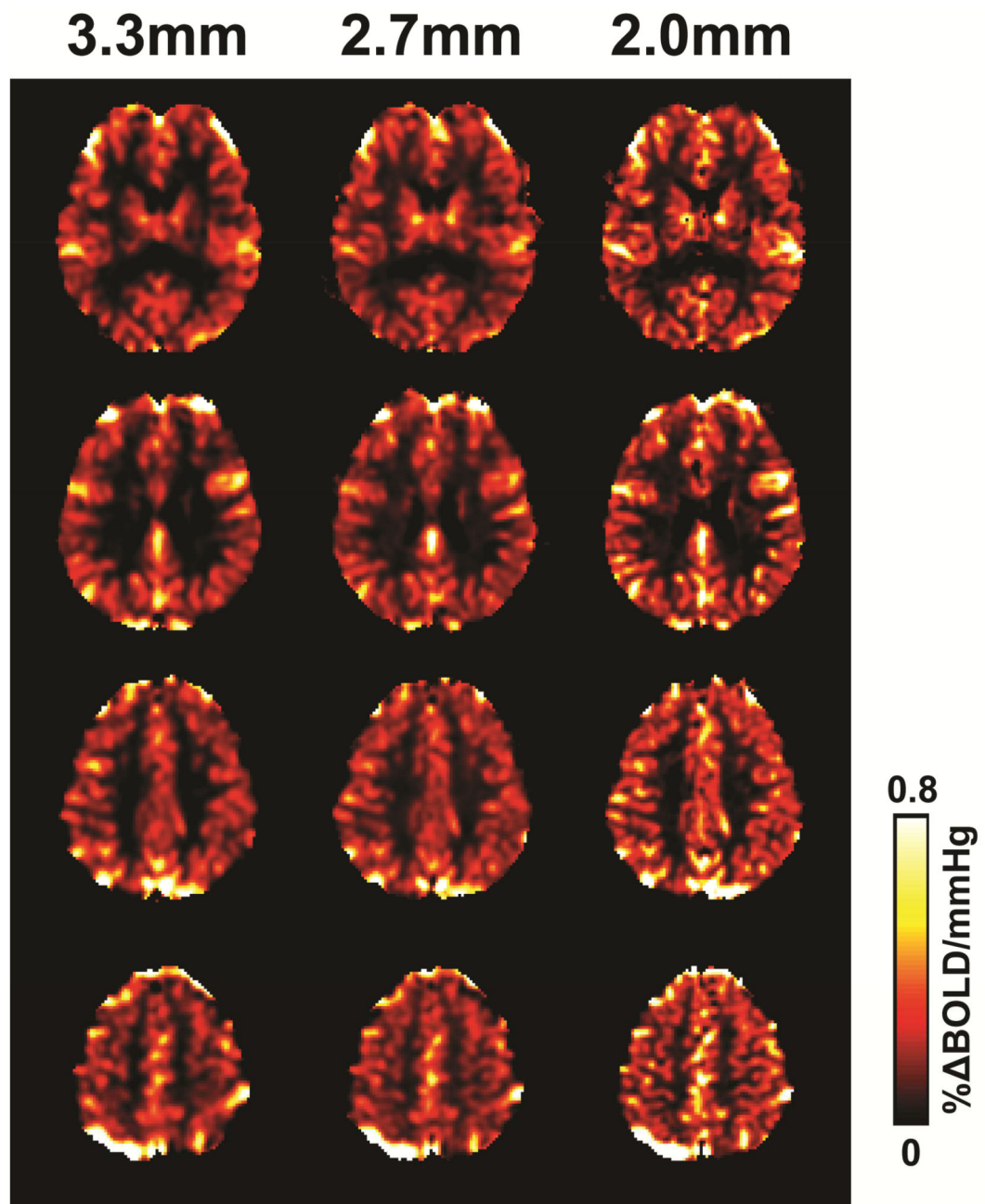Illustration of typical CO2 breathing paradigms.

Figure 5.
CVR maps acquired with different BOLD imaging resolutions in one healthy subject.
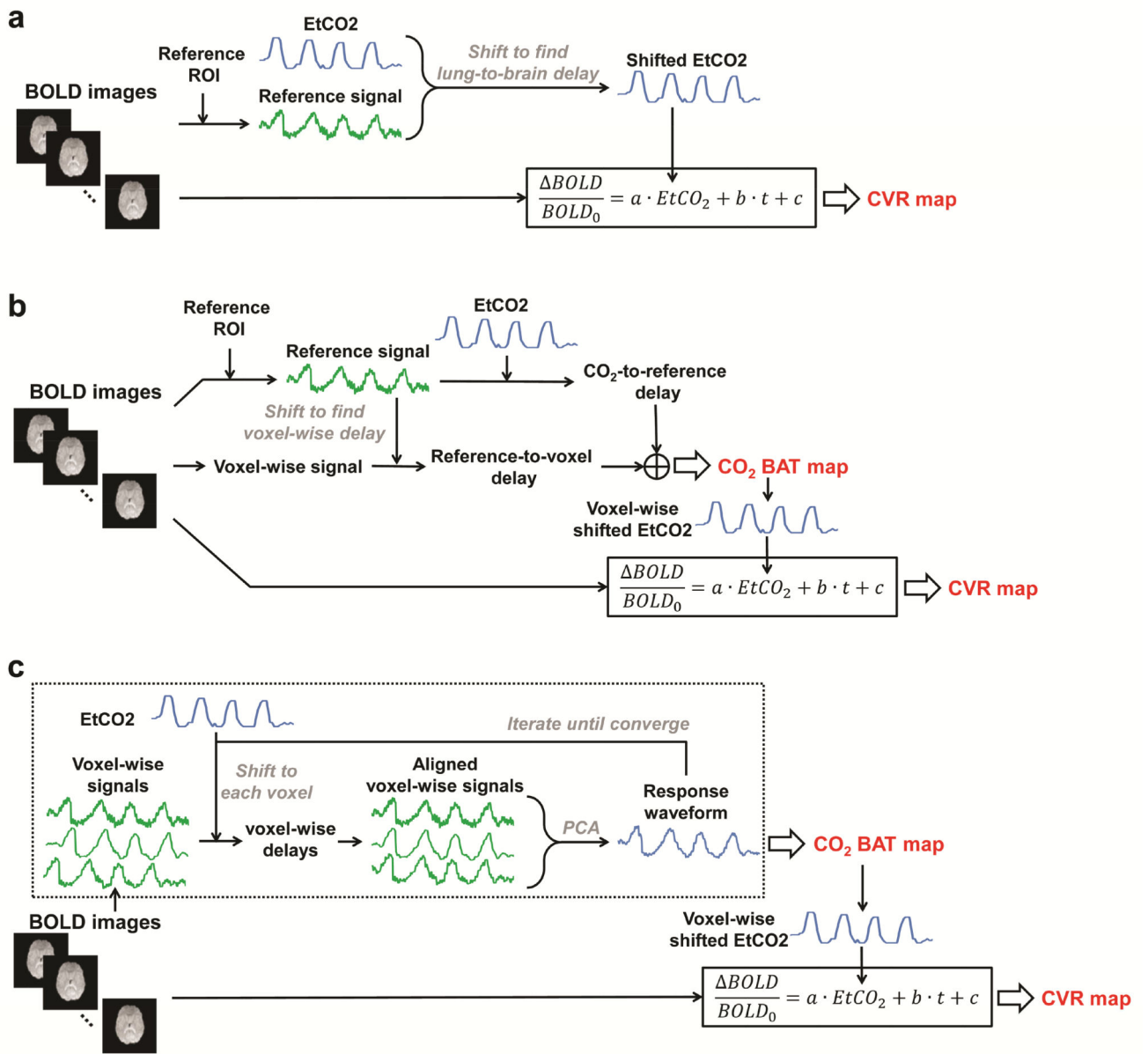5%CO2 inhalation was used. All images were smoothed by a 4mm Gaussian kernel.

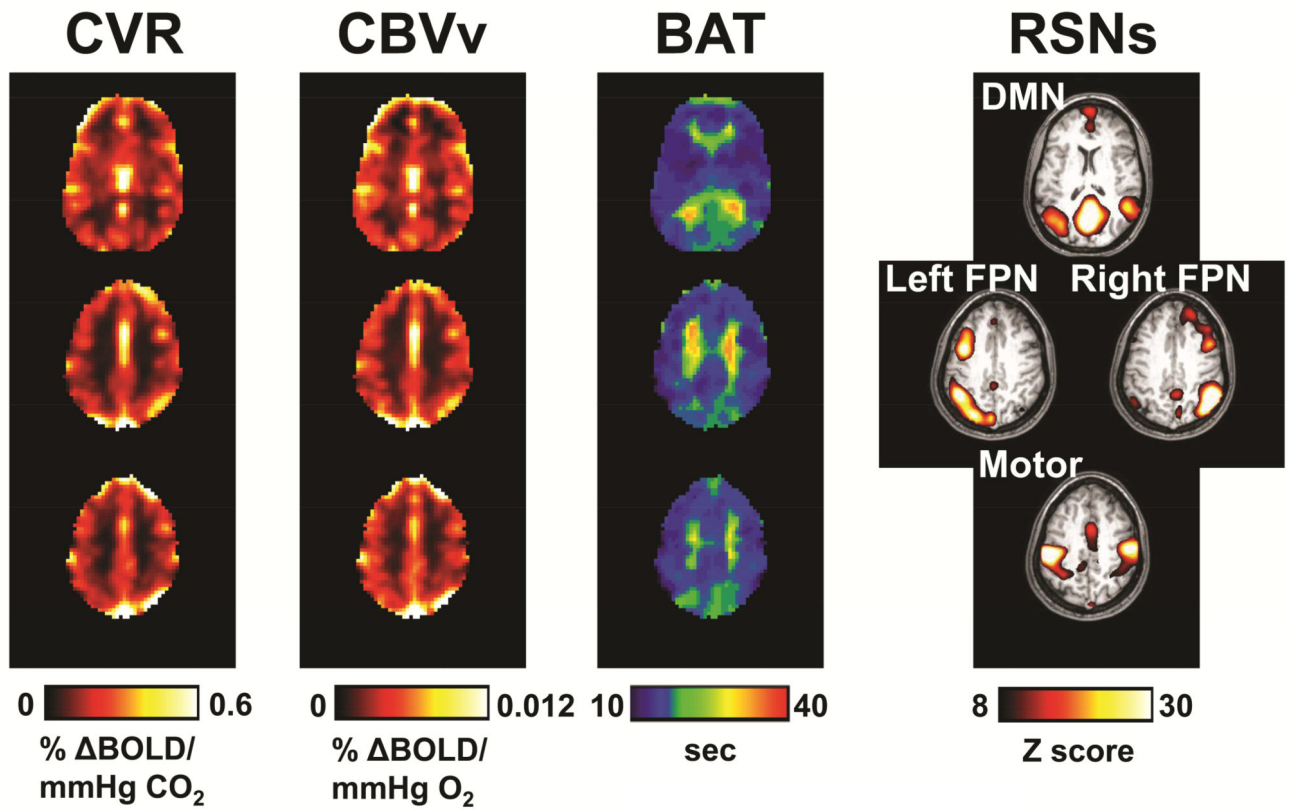**Figure 6.**
Illustration of the CVR data analysis pipelines.

Figure 7.
CVR, CBVv, BAT and functional connectivity networks (FCNs) obtained in a healthy subject (28-year-old female) using concomitant CO2 and O2 inhalation. DMN: Default mode network. FPN: frontal-parietal network.
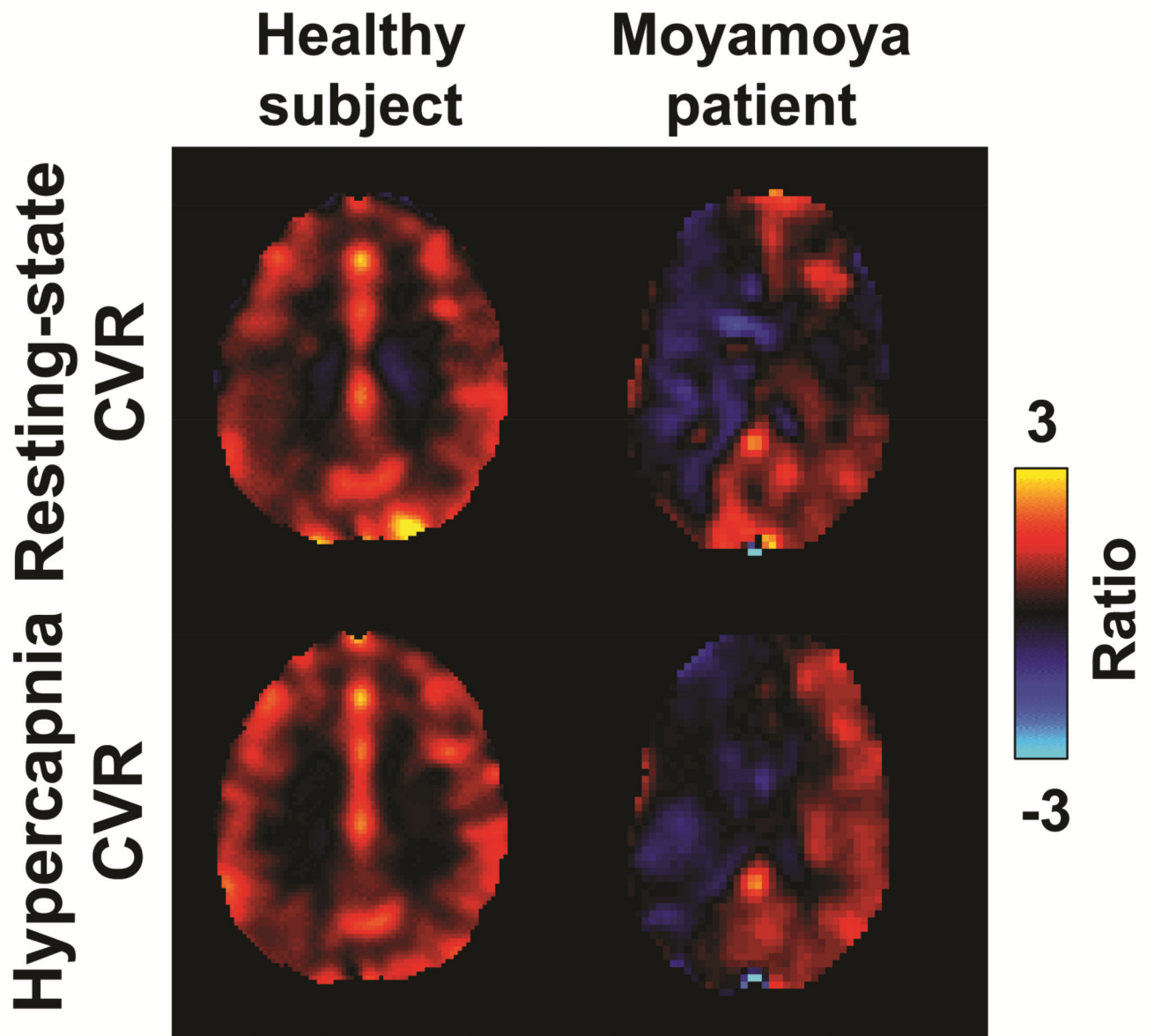
Figure 8.
CVR maps derived from resting-state BOLD data and hypercapnia BOLD data. The healthy subject was a 25-year-old male. The Moyamoya patient was a 24-year-old female with left ICA stenosis.

Table 1

Examples of CVR imaging protocol.

Sequence	Parameters
BOLD	(without SMS) TR=1500–2000 ms, TE=20–30 ms, in-plane resolution 3–4 mm, slice thickness 3–5 mm.
	(with SMS) TR=500–1000 ms, TE=20–40 ms, in-plane resolution 1.8–3.4 mm, slice thickness 1.8–3.4 mm, SMS factor 2–8.
ASL	Pseudo-continuous ASL (PCASL), TR=3.5–7 seconds (depending on background suppression scheme), labeling duration 1500–2000 ms, post-labeling delay 1500–2000 ms, with background suppression, 3D or multi-slice 2D acquisition, in-plane resolution 3–4.5 mm, through-plane resolution 3–7 mm, scan time per breathing state 3–5 min.
PC	In-plane resolution 0.5 mm, slice-thickness 5 mm, non-gated acquisition, scan time for each image 15 s, 2–4 images per breathing state, encoding velocity 40 cm/s for the superior sagittal sinus and 80 cm/s for the internal carotid and vertebral arteries.